THERMAL MODELING AND ANALYSIS OF 193 nm PULSED EXCIMER LASER CALORIMETERS

By

DONGHAI CHEN

A DISSERTATION PRESENTED TO THE GRADUATE SCHOOL
OF THE UNIVERSITY OF FLORIDA IN PARTIAL FULFILLMENT
OF THE REQUIREMENTS FOR THE DEGREE OF
DOCTOR OF PHILOSOPHY

UNIVERSITY OF FLORIDA

2001

ACKNOWLEDGEMENTS

I take this opportunity to express my sincere appreciation to Dr. Zhuomin Zhang for his constant guidance, encouragement and support. He is always helpful in the achievement of my goals and provides a lot of help beyond the research work. I would also like to thank Drs. Jacob Chung, David Hahn, Jill Peterson, and David Tanner for serving on my supervisory committee.

I also gratefully acknowledge Drs. Marla Dowell, Christopher Cromer, and Thomas Scott of the National Institute of Standards and Technology (NIST) for providing valuable information and giving me a chance to work at NIST. I am thankful to my colleagues in the Microscale Thermal Radiation Lab for their assistance. I also extend my thanks to Dr. Ravi Kumar, David Pearson, Ferdinand Rosa, and Jorge Garcia for helping me to improve my English.

I extend my warmest thanks to my parents and dear wife who have been a source of great inspiration and support throughout every challenge in my life.

The final thanks go to the financial supporters of this project: the National Institute of Standards and Technology, and the National Science Foundation.

TABLE OF CONTENTS

page

ACKNOWLDGEMENTS.....ii

ABSTRACT.....v

CHAPTERS

1 INTRODUCTION.....1

2 DEVELOPMENT AND APPLICATIONS OF LASER CALORIMETERS.....5

Brief Review of Calorimeters.....5
CW Laser Calorimeters.....9
Pulsed-Laser Calorimeters.....11
Basic Principles of Laser Calorimetry and the Calibration System.....14

3 THERMAL MODEL AND NUMERICAL SIMULATION METHOD.....23

Previous Study of Laser Heating.....23
Thermal Model Development.....25
Numerical Simulation Method.....30

4 ANALYSIS OF THERMAL MECHANISMS IN VOLUME ABSORBER.....38

Thermal Model of the 193 nm Calorimeter.....38
Three-Dimensional Modeling.....42
Axisymmetric Modeling.....47
Analysis of the Proposed Design.....50

5 MULTIPHOTON ABSORPTION IN VOLUME-ABSORBING GLASS.....67

Introduction.....67
Laser Intensity and Penetration Depth.....68
The Axisymmetric Heating Model.....72
Results of the Numerical Modeling.....75

6 PARAMETRIC STUDY OF EXCIMER LASER CALORIMETERS.....86

The Finite Element Model.....86
Results and Discussion.....89

7 AXISYMMETRIC MODELING OF THE CALORIMETER CAVITY.....99

Axisymmetric Model of the Cavity.....99
Results and Analysis.....102

8 NONEQUIVALENCE ANALYSIS OF LASER CALORIMETERS.....112

Thermal Model of the Cavity.....112
Nonequivalence Analysis.....118

9 SUMMARY AND CONCLUSIONS.....130

Thermal Mechanisms of the Volume Absorber.....130
Parametric Study of the Laser Calorimeter.....132
Nonequivalence of the Laser Calorimeter.....132

APPENDIX NOMENCLATURE.....134

REFERENCES.....138

BIOGRAPHICAL SKETCH.....143

Abstract of Dissertation Presented to the Graduate School
of the University of Florida in Partial Fulfillment of the
Requirements for the Degree of Doctor of Philosophy

THERMAL MODELING AND ANALYSIS OF 193 nm PULSED EXCIMER LASER CALORIMETERS

By

Donghai Chen

May 2001

Chairman: Zhuomin Zhang
Major Department: Mechanical Engineering

This work describes the thermal modeling and analysis of pulsed excimer laser calorimeters at a wavelength of 193 nm. Different thermal models have been developed and the finite element method is employed to perform the thermal modeling of the volume absorber and the cavity in the 193 nm laser calorimeter.

In this work, the heat generation rates in volume absorber and the heat flux on the copper surface have been derived and the finite element method is employed to simulate the space- and time-dependence of temperature in the absorber. A three-dimensional model and an axisymmetric model have been built and used to study the heating effects of single pulse and multiple pulses, respectively. The proposed design, in which the volume absorber is not optically thick, was analyzed under consideration of the reflection and absorption at the interface. The comparison of the present design to the proposed design shows that the accuracy and dynamic range can be improved for the volume

absorber with low absorption coefficient. The two-photon absorption in the volume-absorbing glass is investigated and the results show that the two-photon absorption can compress the volume-absorbing effect to surface absorption with high-power, short-pulse laser irradiation.

The parametric study of excimer laser calorimeter has been performed for pulsed-laser heating, average-power laser heating, and electrical heating using the axisymmetric model in which the volume absorber with small thickness and high absorption coefficient was considered. The maximum temperature is higher for pulsed-laser heating than for electrical heating when the amount of total deposited energy is the same. The equivalence between pulsed-laser heating and average-power laser heating is verified through the axisymmetric modeling of the cavity. A three-dimensional model of the full cavity is employed to predict the calibration factor for laser heating. The nonequivalence of the laser calorimeter is evaluated based on the results of the full cavity modeling. Detailed thermal modeling and analysis of laser calorimeter are provided which help understand the thermal response of the volume absorber and the cavity under laser heating and electrical heating. This work will help improve the future design of pulsed-laser calorimeters.

CHAPTER 1
INTRODUCTION

Excimer lasers have been commercially available since 1975 and are widely used in a number of applications demanding the highest resolution in addition to semiconductor manufacturing, such as micromachining, heat-sensitive materials processing and photorefractive keratectomy (PRK). The most popular wavelengths are 157, 193, 248, 308, and 351 nm. Applications of 248 nm pulsed excimer laser in semiconductor industry led to the construction of calibration system for pulsed-laser energy/power meters at this wavelength.

Calibration technologies for energy/power meters of pulsed excimer laser at the wavelength of 193 nm are motivated by its scientific, industrial and medical applications. In medical applications, such as PRK, 193 nm excimer laser is used to remove tissue precisely from cornea to correct the diopter with the minimum heat effects on surrounding tissue (Pätzel, 1999). The Semiconductor Industry Association roadmap lists 193 nm excimer laser as one immediate candidate for printing feature of 0.18 μm, along with extensions of 248 nm excimer laser (Rothschild et al., 1997). The wavelength change from 248 to 193 nm in photolithographic techniques and other applications requires parallel progress in the calibration technologies. Laser calorimeters, known for their long-term stability and overall accuracy, are widely used to calibrate laser energy/power meters at different wavelength. Hence, it is necessary to build calorimeter

for calibrating energy/power meters of pulsed excimer lasers at 193 nm based on DUV calorimeters at the wavelength of 248 nm (Leonhardt and Scott, 1995).

An isoperibol laser calorimeter consists of an absorbing cavity that is surrounded by a constant-temperature heat sink (West et al., 1972). Laser energy (or power) is absorbed by the cavity and converted into internal energy of the absorbing cavity. The temperature difference between the cavity and the heat sink is a measure of laser energy (or power). Electrical-calibration methods provide a direct comparison between optical and electrical heating thus eliminating the requirement for precise measurements of a calorimeter's thermal properties. Electrical-calibration methods also provide direct traceability to SI units and improve calibration accuracy (West and Churney, 1970). Calorimeters have been designed to operate at specific wavelengths and power/energy levels by the careful selection of absorbing materials for the cavity. Surface absorbers, such as black paint, have been widely used in calorimeters for low power, continuous-wave (CW) measurements. However, surface absorbers are not appropriate for high power pulsed-laser measurements because the high transient temperature gradients produced at the surface can lead to surface damage. For this reason, volume-absorbing materials, which disperse the absorbed energy over a larger volume, are used in calorimeters for pulsed-laser measurements.

It is important to select a volume-absorbing material appropriate for the pulsed excimer laser at 193 nm because the long-term exposure to high peak power output from excimer lasers, a result of high photon energies combined with short pulse widths, causes damage to most conventional optical materials. In addition, the high peak power of the 193 nm pulsed excimer laser can result in a high temperature on the surface of volume

absorber and a nonequivalence between pulsed-laser heating and electrical calibration, which limit the dynamic range and accuracy of calorimeter, respectively. Concerns for these issues are mainly the thermal responses of the volume-absorbing material to pulsed-laser heating and electrical heating, and the uncertainty of the pulsed-laser calorimeter. Therefore, thermal modeling is performed to predict the thermal responses of the volume absorber and the cavity.

In the present study, the main objectives are to understand the heat transfer mechanisms in the volume-absorbing glass with different thickness and absorption coefficients, to evaluate the nonequivalence of the pulsed laser calorimeter. Different thermal model are built using the finite element software ANSYS 5.4-5.6, based on the 193 nm laser calorimeter in which the absorbers are volume-absorbing glass. A three-dimensional model of the volume absorber is used to study the single-pulse heating. An axisymmetric model of the volume absorber is employed to model the multiple-pulse heating, perform the parametric study of excimer laser calorimeters, and investigate the multiphoton absorption in the volume-absorbing glass; an axisymmetric model of the cavity is built for analyzing the difference between the pulsed-laser heating and the average-power laser heating; a three-dimensional model of the full cavity is developed to predict the nonequivalence of the 193 nm pulsed-laser calorimeter.

The organization of this dissertation is as follows. Chapter 2 presents a review of the development and applications of laser calorimeters. The thermal model of volume-absorbing glass irradiated by laser pulse and a brief review of the work related to laser heating are described in Chapter 3. The thermal mechanisms of the volume-absorbing glass under 193 nm pulsed-laser irradiation and the influence of the absorption coefficient

on the thermal response of the glass are analyzed in Chapter 4. Multiphoton absorption in the volume-absorbing glass under 193 nm pulsed-laser irradiation is presented in Chapter 5. The parametric study of excimer laser calorimeters is described in Chapter 6. The equivalence between the pulsed-laser heating and the average-power laser heating is analyzed in Chapter 7. The nonequivalence of the 193 nm pulsed-laser calorimeter is predicted in Chapter 8. Finally, summary and conclusions are given in Chapter 9.

CHAPTER 2
DEVELOPMENT AND APPLICATIONS OF LASER CALORIMETERS

Calorimeters have been designed at different operation modes and used for measuring the heat involved in physical and chemical processes for more than two hundreds years. A requirement for all calorimeters is that they must quantitatively measure the changes of material property caused by exchanged heats. After a brief review of calorimeters, the development and applications of laser calorimeters are discussed in this chapter.

Brief Review of Calorimeters

Calorimeters are the instruments used for measuring the heat involved in a change of phase, temperature, pressure, volume, chemical composition and any other material property (Himminger and Höhne, 1984; McCullough and Scott, 1968). Since the eighteenth century, calorimetry has been developed and various calorimeters have been built for different purpose. For example, Lavoisier designed an ice calorimeter in 1784, Hess used an effective reaction calorimeter in 1839, and Bertholet invented a bomb calorimeter in 1885 (Brown, 1969). In recent years, advances in electronics have continuously opened new application horizons for calorimeters, new materials have successfully widened the dynamic range of calorimeters, and automatic data processing

has largely improved their accuracy. Developments during the past few centuries have added the calorimeter to the category of precision instruments and extended the application range of calorimeters down to absolute zero and up to temperatures above 1000 °C. Although the use of the calorimeter as the essential measurement instrument of heat in experimental thermodynamics and thermochemistry requires a wide range of design, it is basically classified as *isothermal*, *adiabatic*, *isoperibol* and *scanning* calorimeters according to the operating mode.

In isothermal calorimeters, the measuring system is at the same constant temperature as the surroundings, $T_M = T_S$ = constant, as shown in Fig. 2-1. The thermal resistance R_{th} between the measuring system and surroundings must be very small for achieving the isothermal operation. The phase change is utilized to maintain the constant temperature in many isothermal calorimeters. For example, the solid-phase change was used in the ice calorimeter and the liquid-vapor change is also used by other calorimeters. The electrical heating is another method used to maintain the constant temperature by balancing the addition or removal of heat. The electrical compensation was used in the isothermal twin calorimeter described by Duane (Himminger and Höhne, 1984). The isothermal calorimeter has occupied a predominant position in calorimetry before the tremendous improvement of the adiabatic shield.

The adiabatic operation mode can also be achieved in calorimeters under ideal conditions. The calorimeter of this type is subsequently called an adiabatic calorimeter. As shown in Fig. 2-1, the thermal resistance R_{th} between the measuring system and surroundings should be "infinitely large" and the surroundings must be constantly controlled to the same temperature as the measuring system, $T_M = T_S$. The "infinitely

large" thermal resistance means that the heat conduction, convection and radiation between surroundings and the measuring system must be insulated in the best possible way. It is easier to realize the insulation for the low-temperature adiabatic calorimeter (10-300 K) than for the high-temperature adiabatic calorimeter (300-800 K) because the rate of radiation heat transfer increases greatly at high temperatures. The difficulties for the high-temperature calorimetry have been generally discussed by Kingery (1959). The adiabatic calorimeter shows considerable advantage for measurements of the heat released at a slow or moderate rate because the surroundings and the measuring system are easily controlled at the same temperature. However, it is difficult to satisfy the same temperature requirement for the surroundings with large area and the sudden temperature change of the measuring system. The accuracy of adiabatic calorimeter depends mainly on the effectiveness of adiabatic. The adiabatic condition in modern calorimeters is established only by the electronic control.

In the isoperibol calorimeter, the surrounding is maintained at a constant temperature, T_S = constant, which is different from T_M, the temperature of the measuring system (Himminger and Höhne, 1984; Skinner, 1962). The thermal resistance R_{th} between the surroundings and the measuring system is finite, unlike the very small resistance in isothermal calorimeters and infinitely large resistance in adiabatic calorimeters. Hence, it is easier to realize the isoperibol operation than isothermal and adiabatic operations. Since the heat flux between the surroundings and the measuring system is a function of the temperature of the measuring system, it can be reduced through decreasing the temperature rise of the measuring system. The energy loss of the measuring system can be determined in the electrical calibration. Hence, the magnitude

of energy loss in an isoperibol calorimeter is not very important for the accuracy, but it can influence the sensitivity of calorimeter. Laser calorimeters are built with the isoperibol operation mode.

The scanning operation includes scanning of surroundings, adiabatic scanning, and isoperibol scanning. The typical calorimeter with the scanning of surroundings is the heat flux calorimeter. In the heat flux calorimeter, the measuring system is connected to the surroundings by a solid body with a defined thermal resistance. The heat can be transferred from the measuring system to the surroundings only by the conduction through the solid body. Convection and radiation are kept as small as possible. The temperature of surroundings follows that of the measuring system with a time lag in the measurement. When steady state is established, the heat flux through the solid body can be determined by the temperature difference between the measuring system and the surroundings. The adiabatic scanning operation is used in differential power scanning calorimeters, in which the temperature of the measuring system is controlled to the same temperature as the surroundings. In the calorimeters with isoperibol scanning operation, there are actually two separate measuring systems. Each measuring system is brought to the temperature identical to the other one by the controlled heater and the temperature of the surroundings is kept constant.

Based on these four operating modes, various calorimeters have been built for measuring the heat in reacting systems and non-reacting systems. With the development of electronics and materials, the application range of the calorimeter has been extended to the optical energy measurement, especially for measuring laser power and energy. Laser calorimetry is to compare the laser outputs directly to the electrical standards (West et al.,

1972). Hence, the application of laser calorimetry reduces the number of steps to determine the thermal properties of materials. Another advantage of laser calorimetry is that it can be used to measure the power and energy of both continuous-wave (CW) lasers and pulsed lasers.

CW Laser Calorimeters

Ever since the laser was demonstrated in 1960, it has been widely used in scientific, industrial, and medical areas. With its extensive application, the accurate measurement of laser power and energy becomes more and more important. Hence, laser calorimeters for measuring the power and energy of lasers are developed. This type of calorimeter operates at constant-temperature surroundings and belongs to the category of isoperibol calorimeter (West and Churney, 1970). Over the past 30 years, C-series, K-series, Q-series and QUV calorimeters have been built at the National Institute of Standards and Technology (NIST) and used as national reference standards for calibrating laser power and energy meters (Scott, 1988; Leonhardt and Scott, 1995).

The C-Series Laser Calorimeters

The C-series laser calorimeters operate at or above room temperature and measure laser energy from the temperature change of the receiver caused by the absorption of optical radiation. As shown in Fig. 2-2, the receiver in the C-series calorimeter consists of an absorbing cavity and a shield cavity. The absorbing cavity is a cylindrical cavity made of thin copper plate, whose inner surface is coated with flat black paint and outer surface is gold plated. The electrical heater is attached to the outer surface of the absorbing cavity. The shield cavity surrounds the absorbing cavity and they are

connected at the middle section. The shield cavity is made of gold-plated copper to reduce the radiative heat transfer and the convection heat transfer is eliminated through creating a vacuum inside the calorimeter. The receiver is suspended in the temperature-controlled heat sink by thermocouples. Laser energy and electrical energy are absorbed by the absorbing cavity and then its internal energy is transferred to the shield cavity by heat conduction. The temperature rise of the shied cavity is measured by thermocouples.

The C-series calorimeters were used for measuring the radiation energy of continuous wave lasers. The dynamic ranges of C-series calorimeters are from 0.1 mW to 2 W in power and 0.03 to 30 J in energy (Zhang et al., 1996; West and Case, 1974). The absorbing wavelength range of black paint is from 0.4 to 22 μm. However, the usable wavelength range for C-series calorimeter is from 0.4 to 2 μm limited by the window. The maximum beam size limited by the apertures is 2 cm in diameter. The total uncertainty of the C-series calorimeter is 0.34% (Scott, 1988).

The K-Series Laser Calorimeters

The K-series laser calorimeters including K1 series and K2 series were built to measure the output of a laser whose power level is beyond the dynamic range of the C-series calorimeter. K2-series calorimeter is capable of measuring the energy of lasers in the power range from 0.2 to 40 W (Scott, 1988). As shown in Fig. 2-3, the thin-wall cavity is made of copper; its inside surface is coated with black paint; the sensing bridge and electrical heater are attached to the outside surface of the sidewall and the bottom of the cavity, respectively. The usable wavelength range is extended from 0.4 to 22 μm

because there is no window limit. The total uncertainty is 1.19% for the K2-series calorimeter.

The dynamic range of K1-series calorimeter is from 5 to 1000 W (Scott, 1988). The structure of the K1-series calorimeter is much similar to that of the C-series calorimeter. There is no window in the K1-series calorimeter, but it has a mirror at the back of the cavity. This mirror is used to decrease the incident laser power by spreading the laser radiation to the side surface of the cavity. Hence, the laser energy density is reduced before the laser beam reaches the bottom of the cavity to keep it from getting damaged. The total uncertainty is 1.26% for the K1-series calorimeter. The wavelength range is from 0.4-22 μm, but it is only used at 10.6 μm.

Pulsed-Laser Calorimeters

The Q-Series Pulsed-Laser Calorimeters

The Q-series pulsed-laser calorimeters were designed for measuring the pulsed laser energy. Because the energy density of a laser pulse is usually high enough to damage the black paint, surface-absorbing materials are no longer applicable to absorb its energy. Hence, volume-absorbing glass is used in the cavity of Q-series calorimeters shown in Fig. 2-4. A glass plate with a thickness of 2 mm is expoxied on the inner surface of the cavity bottom at an angle of 30° with the vertical direction. Another glass plate with the thickness of 1 mm is placed at the location of the first Fresnel reflection if the energy density at this location exceeds the damage threshold of black paint. The electrical heater is epoxied to the outside surface of the cavity bottom and thermocouples are attached to cavity and heat sink.

The energy range of the Q-series calorimeter is from 0.4 to 15 J and the maximum energy density per pulse is 3 J/cm^2 (Franzen and Schmidt, 1976). An aperture of 32 × 32 mm^2 limits the laser beam up to 1 cm in diameter and the minimum pulse width is 20 ns. The wavelength range determined by the spectral absorption coefficient is from 0.5 to 1.2 μm, but it is only used at the wavelength of 1.06 μm. The total uncertainty is 0.85% for the Q-series calorimeter.

The QUV Pulsed-Laser Calorimeters

The QUV calorimeters (QUV-1 and QUV-2) are designed to measure the energy of excimer laser pulses at the wavelength of 248 nm (Leonhardt, 1998; Leonhardt and Scott, 1995). The maximum pulse energy of the excimer laser source is 400 mJ and the pulse width is approximately 30 to 35 ns. The repetition rate of the pulse can be up to 100 Hz. The irradiance of excimer laser pulse at 248 nm is potentially high and non-uniform, and can cause fluorescence and damage the surface-absorbing materials. Hence, two colored glass filters with volume-absorbing capability are bonded with thermally conducting epoxy to the back of each cavity. The structure of the QUV calorimeter is the same as that of the Q-series calorimeter differing only in the volume-absorbing material. The thickness of each glass plate is kept the same as the Q-series calorimeter. However, the absorption coefficient of the colored glass filter is 33.2 cm^{-1}. More than 99% of laser energy is absorbed inside the glass and the heat flux on the copper surface is very small.

QUV calorimeters are reference standards for 248-nm excimer laser energy at NIST. Their dynamic ranges are from 0.6 to 15 J. The QUV calorimeter calibration system is not used directly to calibrate the excimer laser source, but to calibrate the

meters for excimer laser power and energy at the wavelength 248 nm. The calibration range is from 400 μW to 7.5 W for laser-power meters and from 80 μJ to 150 mJ for laser-energy meters. The total measurement uncertainty ranges from 1.6 to 2%.

The 193 nm Pulsed-Laser Calorimeter

The 193 nm pulsed-laser calorimeter has been built largely based on the design of QUV calorimeter and the calibration system is in construction at NIST. This type of calorimeter is designed for measuring the pulsed excimer laser energy at the wavelength of 193 nm. The calibration technology at 193 nm is motivated mainly by the development of lithography using 193 nm ArF excimer laser in the semi-conductor industry. The average energy of excimer laser pulse at 193 nm is 100 mJ to 15 J, the beam diameter is up to 1 cm and the repetition rate of pulse can be up to 100 Hz. Because the average energy of pulse can be up to 15 J, the maximum energy density per pulse depends on the beam size. The cavity in the 193 nm calorimeter is made up of thin copper plate and its structure is the same as that in Q-series calorimeter. Two volume absorbers are placed in the cavity and an electrical heater is epoxied to the outside surface of the bottom plate. The selected volume-absorbing glass must be appropriate to absorb the excimer laser energy at 193 nm without damage and the different thickness should be used for the glass with different absorption coefficient. The 193 nm calorimeter has just been designed and built at NIST. The dynamic range, accuracy and heat transfer mechanisms in the calorimeter need to be understood. Hence, thermal modeling and analysis of the 193 nm calorimeter have been performed, and the thermal model and modeling results are discussed in the following chapters.

Basic Principles of Laser Calorimetry and the Calibration System

Laser calorimeter operating in a constant-temperature surrounding is called isoperibol calorimeter. The usual theory of calorimeter with isoperibol operation was derived under the assumption of uniform temperature in the measuring system (White, 1928). This assumption is invalid for laser calorimeter with a non-uniform temperature cavity. The theory of isoperibol calorimetry for laser power and energy measurements is derived by West and Churney (1970) and is generally used for the laser calorimeters.

Basic Principles of Laser Calorimetry

In laser calorimeters, laser radiation is absorbed by the absorber in the cavity and converted to thermal energy. The thermal energy is transferred to the back of the cavity and quickly diffuses in the cavity wall. Part of the thermal energy becomes internal energy in the cavity and causes the temperature to increase; part of the energy is lost to the surroundings by conduction, convection and radiation. The temperature of the cavity is measured by a thermopile as voltage output. The voltage output is assumed to be linearly related to the temperature which can be expressed as a series of exponential functions. At some time after energy injection, a single exponential function can describe the output temperature by neglecting the higher order functions. The exponential equation is expressed as

$$T(t) - T_0 = (T_I - T_0)e^{-\eta(t-t_I)} \qquad (2\text{-}1)$$

where t_I is the initial time of the single exponential description of output, T_I is the temperature at time t_I, T_0 is the ambient temperature, and η is the cooling constant.

The output of the thermopile during one measurement is shown in Fig. 2-5. Energy injection starts at t_d and ends at t_e; the output temperature of the thermopile reaches the peak value at t_p. Times t_1 and t_2 occur when the temperature output can be described exactly by a single exponential decay function, hence, they should be long enough after the energy injection. The period from t_1 to t_d is the initial rating period, the time from t_p to t_2 is the relaxation period, and the time from t_2 to t_3 is the final rating period. According to the first law of thermodynamics, the energy absorbed by the cavity is equal to the sum of the internal energy increase of the cavity and the energy loss to the environment. The internal energy increase is proportional to the quantity $(T_2 - T_1)$ by the constant K and the energy loss is proportional to the following quantity by the same proportionality constant:

$$\eta \int_{t_1}^{t_2} (T(t) - T_0) dt \tag{2-2}$$

Hence, the total energy absorbed by the cavity can be described as

$$E = K\left[(T_2 - T_1) + \eta \int_{t_1}^{t_2} (T(t) - T_0) dt \right] \tag{2-3}$$

where the proportionality constant K is termed as the calibration factor, and T_1 and T_2 are temperatures at times t_1 and t_2, respectively. Under the uniform temperature assumption, K is the heat capacity of the calorimeter cavity. However, a correction coefficient for the actual non-uniform distribution must be involved in it. Hence, the calibration factor K is a combination of the heat capacity of the cavity and the correction coefficient for the non-uniform temperature distribution on the surfaces of the cavity. Unknown parameters η, T_0, T_1 and T_2 are found by using Eq. 2-1 in the neighboring region of T_1 and T_2. The calibration factor K is determined by electrical calibration with a known energy and used

for calculating the laser energy. Hence, the nonequivalence between electrical heating and laser heating is very important for the accuracy of laser calorimeter.

The Calibration System

A calorimeter calibration system for measuring laser energy and comparing power or energy meters to the reference standard is shown in Fig. 2-6. The energy injection is controlled for a predetermined interval by the timed shutter. When a laser beam is incident on the beamsplitter, the specular reflection from the first surface of the beamsplitter is directed into a test meter and the main transmitted beam goes to the reference calorimeter. The positions of reference calorimeter and test meter can be interchanged. The known ratio of the transmitted energy to the reflected energy from the beamsplitter is used in conjunction with the energy measured by the reference calorimeter to calculate the input energy of the test meter. The output of the test meter is compared with the calculated input energy and the accuracy of the test meter is evaluated.

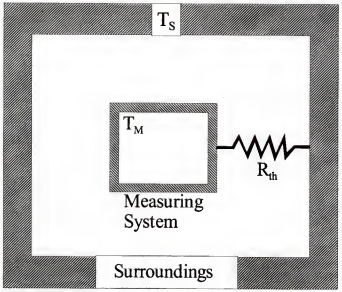

R_{th}: Thermal resistance
T_S: Temperature of surroundings
T_M: Temperature of measuring system

Figure 2-1. Schematic of a calorimeter.

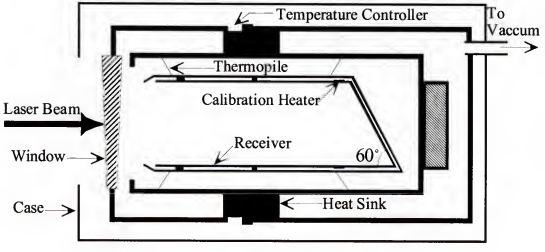

Figure 2-2. C-series laser calorimeter (West and Case, 1974).

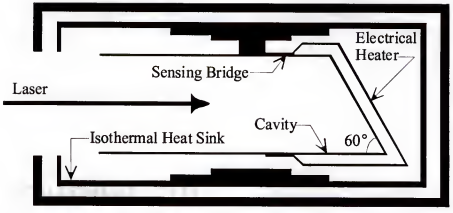

Figure 2-3. K2-series laser calorimeter (Scott, 1988).

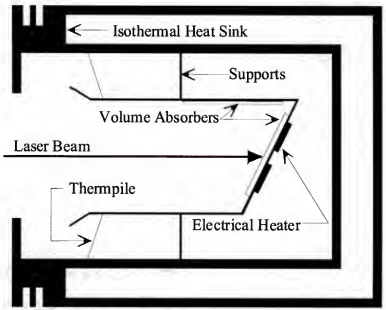

Figure 2-4. Q-series pulsed laser calorimeter (Franzen and Schmidt, 1976).

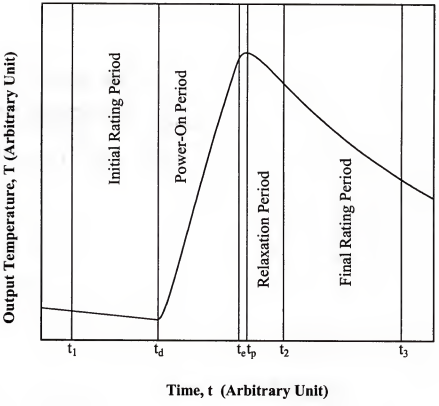

Figure 2-5. Calorimeter output temperature as a function of time.

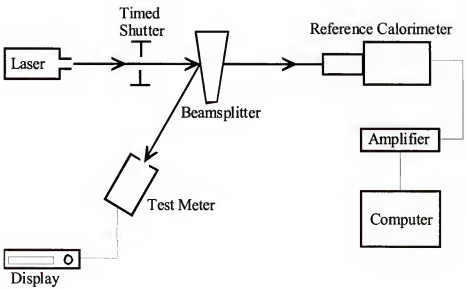

Figure 2-6. Calorimeter measurement system.

CHAPTER 3
THERMAL MODEL AND NUMERICAL SIMULATION METHOD

This study is based on the volume-absorber in the 193 nm pulsed-laser calorimeter. A thermal model of volume-absorbing glass under pulsed-laser heating has been developed. The finite element analysis method is introduced and the applicability of Fourier's heat conduction equation is discussed.

Previous Study of Laser Heating

Lasers have been widely used in the semiconductor industry and advanced material processing. Laser-solid interaction has attracted the considerable interest of many researchers. Different models and techniques have been developed and used to study the thermal characteristics related to the laser-solid interaction.

McGahan et al. (1992) derived the exact solution of the heat conduction equation of laser heating multilayers from a local Green's function theory. Grigoropoulos et al. (1993) modeled the pulsed-laser irradiation on thin silicon layers; they assumed a uniform intensity in the laser beam, an equilateral-triangular temporal shape of laser pulse, and a continuous exponential decay of the radiation intensity in the silicon layer. El-Adawi et al. (1995) studied the laser heating of a two-layer system with constant surface absorption using the Laplace integral transform method and obtained the exact solutions of temperature profiles in the thin film and substrate. Xu et al. (1995) used one-

dimensional conductive heat transfer model to study the heat transfer in the melting of thin polysilicon layers heated by KrF excimer laser. Angelucci and Bianco (1997) analyzed the thermal transient process of thin-film multilayers heated by the nanosecond pulses of Nd-YAG laser. In these studies, the laser beam is perpendicularly incident and the incident intensity is assumed uniform; one-dimensional heat conduction is considered in the solid near the center of the laser beam; the radiation and convection on the heating surface are neglected.

Xu and Song (1997) studied the radiative transfer in plasma induced by laser pulses. In their study, the excimer laser transfer in the plasma layer is considered a one-dimensional radiative transfer process. Fushinobu et al. (1996) investigated the heat transfer characteristics in polymers with excimer laser irradiation using one-dimensional and three-dimensional models. They assumed a constant heat flux is supplied to one surface during laser heating process and the adiabatic condition is applied after the heating process. Ganesh and Faghri (1997) performed the thermal modeling for laser drilling process, in which an axial-symmetric model is used and the laser beam intensity is a Gaussian function of space and time.

Qiu and Tien (1992; 1994) performed an extensive investigation of radiation-metal interactions. They treat the radiation-metal interaction as a coupled two-step process: the absorption of photon energy by electrons and the subsequent heating of the metal phonon through the electron-phonon collisions, and developed a parabolic two-step model based on the conventional Fourier heat conduction model (parabolic one-step model). The temperature profiles of metals during the heating of short laser pulses are modeled using these two models. The order of pulse width is from femtoseconds to

nanoseconds. Experiments with a higher temporal resolution are performed to investigate the thermal mechanisms in multi-layer metals during short-pulse heating (Qiu et al., 1994). The modeling predictions are compared with the experimental results and an application regime of laser heating models for gold is given.

Thermal Model Development

The schematic of the cavity made up of thin copper plate in the 193 nm calorimeter is shown in Fig. 3-1. In the measurement, laser beam hits the surface of the volume-absorbing glass at the back of the cavity at an incident angle of 30° and its energy is absorbed mainly in this glass plate. The absorbed laser energy is regarded as internal heat sources in the glass. Hence, a thermal model of volume-absorbing glass under pulsed-laser heating has been developed and the heat generation rate in the glass has been derived with only one-photon absorption.

Model of Laser Pulse

Gaussian distributions are used to model the excimer laser pulse with respect to the temporal and spatial distributions. As shown in Figs. 3-2 and 3-3, the power of the laser pulse is assumed to be a Gaussian function of time and the intensity of laser pulse (defined as the radiant power per unit area normal to the laser beam) is assumed to be a Gaussian function of space. According to the Gaussian shape function (Svelto, 1998), the power P(t) and the intensity I(r, t) of pulse can be expressed as

$$P(t) = P_m e^{-4\ln(2)\cdot(t-t_m)^2/\tau_p^2} \tag{3-1}$$

$$I(r,t) = I_m(t) \cdot e^{-4\ln(2)\cdot r^2/D^2} \tag{3-2}$$

where P_m and $I_m(t)$ are the peak power and the peak intensity of laser pulse, respectively; t_m is the time at peak power; τ_p is the full width at half maximum (FWHM) pulse width and D is the FWHM beam diameter. A single pulse is assumed to be from $-\infty$ to $+\infty$ in time domain and infinite in space domain. From the relation between the pulse energy Q and the power, $Q = \int_{-\infty}^{+\infty} P(t)dt$, the peak power can be determined as

$$P_m = \frac{2\sqrt{\ln(2)}\cdot Q}{\tau_p\sqrt{\pi}} \tag{3-3}$$

Substituting Eq. (3-3) in-to Eq. (3-1), the power of laser pulse is

$$P(t) = \frac{2\sqrt{\ln(2)}\cdot Q}{\tau_p\sqrt{\pi}} \cdot e^{-4\ln(2)\cdot(t-t_m)^2/\tau_p^2} \tag{3-4}$$

The peak intensity is derived from the relation between the power and intensity:

$$P(t) = \int_0^{+\infty} I(r,t)\cdot 2\pi r dr \tag{3-5}$$

Substituting Eqs. (3-2) and (3-4) in-to Eq. (3-5) and solving for $I_m(t)$,

$$I_m(t) = \frac{8[\ln(2)]^{3/2}\cdot Q}{\pi^{3/2}\cdot\tau_p\cdot D^2} \cdot e^{-4\ln(2)\cdot(t-t_m)^2/\tau_p^2} \tag{3-6}$$

Substituting Eq. (3-6) in-to Eq. (3-2), the intensity in the cross section of the laser beam is obtained as

$$I(r,t) = \frac{8[\ln(2)]^{3/2}\cdot Q}{\pi^{3/2}\cdot\tau_p\cdot D^2} \cdot e^{-4\ln(2)\cdot(t-t_m)^2/\tau_p^2} \cdot e^{-4\ln(2)\cdot r^2/D^2} \tag{3-7}$$

When the laser beam is incident on a x-y plane (z = 0) at an incident angle θ_1 and it is tilted only in the x direction as shown in Fig. 3-4, the intensity I(x, y, 0, t) can be expressed as

$$I(x,y,0,t) = I(r,t) \tag{3-8}$$

where r is the cylindrical coordinate in the cross section of the laser beam, $r = \sqrt{x^2 \cos^2\theta_1 + y^2}$. The incident intensity of the laser beam is proportional to the pulse energy Q and inversely proportional to the pulse width τ_p and the square of D. Although the intensity is derived under the assumption of infinite domains, it is accurate for the finite domains because of the assumption of Gaussian distributions in time and space.

Model of Volume-Absorbing Glass

The schematic of the thermal model of volume-absorbing glass is shown in Fig. 3-5. The laser beam is incident on the glass surface (z = 0) at an angle θ_1 and the incident intensity I(x, y, 0, t) is given by Eq. (3-8). Part of the laser energy is reflected from the surface with the reflectance R_g, but most of laser energy is transmitted into the glass at a refractive angle of $\theta_2 = \sin^{-1}(\frac{n_{air}}{n_g}\sin\theta_1)$. The transmittance is equal to $(1 - R_g)$. The transmitted intensity $I_t(x, y, z, t)$ on the glass surface (z = 0) is derived as

$$I_t(x,y,0,t) = (1-R_g)\cdot\frac{\cos\theta_1}{\cos\theta_2}\cdot I(x,y,0,t) \tag{3-9}$$

The absorption of laser energy in the glass is described by the Beer-Lambert law. Thus, the intensity $I_t(x, y, z, t)$ at the point (x, y, z) in the glass can be expressed as

$$I_t(x,y,z,t) = I_t(x_0,y_0,0,t)\cdot e^{-a\cdot\ell} \tag{3-10}$$

where $I_t(x_0, y_0, 0, t)$ is the transmitted intensity at the point $x_0 = x + z\cdot tg\theta_2$ and $y_0 = y$ on the glass surface ($z = 0$); $a = 4\pi\kappa_g/\lambda$ is the absorption coefficient of the glass at the wavelength λ; ℓ is the path length, which is related to z by $\ell = z/\cos\theta_2$. The energy of the laser beam transmitted on the glass surface is absorbed in the glass and the absorbed energy is considered as the internal heat source. At the point (x, y, z), the transmitted intensity is obtained based on Eqs. (3-7), (3-8), (3-9), and (3-10); the heat generation rate $\dot{q}_1(x,y,z,t)$ is subsequently derived as (Chen and Zhang, 2000).

$$\dot{q}_1(x,y,z,t) = C_1\cdot e^{-(t-t_m)^2/\tau^2}\cdot e^{-r^2/b^2}\cdot e^{-a\cdot z/\cos\theta_2} \tag{3-11}$$

In Eq. (3-11), $r = \sqrt{(x + z\cdot\tan\theta_2)^2\cdot\cos^2\theta_1 + y^2}$ is the distance between the beam line that reaches the point (x, y, z) and the central line of the laser beam in the air, $D = 2b\sqrt{\ln 2}$ is the FWHM beam diameter, $\tau_p = 2\tau\sqrt{\ln 2}$ is the FWHM pulse width, t_m is the time at which the power is maximum, and

$$C_1 = \frac{aQ(1-R_g)\cos\theta_1}{\pi^{3/2}b^2\tau\cos\theta_2} \tag{3-12}$$

The derived heat generation rate equation can be used for investigating the thermal mechanisms in volume-absorbing materials for laser heating. When the incident angle and the refractive angle are equal to zero, the heat generation rate is simplified to that of the case of normal laser incidence.

If the glass is optically thick with more than 99% of the transmitted energy absorbed in the glass, the intensity on the glass-copper interface is small. Hence, the surface heating and reflected energy on the surface of copper are neglected. If the glass is not optically thick, some of the transmitted energy can reach the interface between glass and copper, part of them is absorbed on the copper surface, and the other is reflected back into the glass as shown in Fig. 3-5. The reflected energy causes an additional heat generation rate in the glass. For any point (x, y, z) at the path of the reflected laser beam, the path length, ℓ, from the point (x_0, y_0, 0) at the path of the corresponding incident laser beam to this point is $(2L_1 - z)/\cos\theta_2$. The coordinate relations between (x_0, y_0, 0) and (x, y, z) are $y_0 = y$ and $x_0 = x + (2L_1 - z)\cdot\tan\theta_2$. Following the same method as $\dot{q}_1(x, y, z, t)$ and considering the reflectance of the copper surface, the additional heat generation rate $\dot{q}_2(x, y, z, t)$ in the glass is derived as

$$\dot{q}_2(x, y, z, t) = C_2 \cdot e^{-(t-t_m)^2/\tau^2} \cdot e^{-r^2/b^2} \cdot e^{-a\cdot(2L_1 - z)/\cos\theta_2} \qquad (3\text{-}13)$$

where $r = \sqrt{[x + (2L_1 - z)\cdot\tan\theta_2]^2 \cdot \cos^2\theta_1 + y^2}$ and the constant C_2 is defined as

$$C_2 = \frac{aQR_c(1 - R_g)\cos\theta_1}{\pi^{3/2} b^2 \tau \cos\theta_2} \qquad (3\text{-}14)$$

where R_c is the reflectance of the copper surface. The energy absorption on the surface of copper causes a surface heating flux. The incident intensity of laser at the point (x, y, L_1) can be obtained from Eq. (3-10) and the heat flux $q''(x, y, L_1, t)$ on the copper surface is derived as

$$q''(x, y, L_1, t) = C_3 \cdot e^{-(t-t_m)^2/\tau^2} \cdot e^{-r^2/b^2} \cdot e^{-a\cdot L_1/\cos\theta_2} \qquad (3\text{-}15)$$

where $r = \sqrt{(x + L_1 \cdot \tan\theta_2)^2 \cdot \cos^2\theta_1 + y^2}$ and the constant C_3 can be expressed as

$$C_3 = \frac{Q(1-R_g)(1-R_c)\cos\theta_1}{\pi^{3/2} b^2 \tau} \tag{3-16}$$

The additional heat generation rate $\dot{q}_2(x,y,z,t)$ and the surface heat flux $q''(x,y,L_1,t)$ are considered in the studying of the heat transfer characteristics in the glass with low absorption coefficient.

Numerical Simulation Method

Heat Conduction Equation

The application of the parabolic Fourier's heat conduction equation in a short-pulse laser heating process is subject to question. Wave-type propagation of heat, instead of diffusion, has been proposed under thermal wave theory, which results in the one-step hyperbolic heat conduction model for short-laser heating process (Özisik and Tzou, 1994). The two-step model and hyperbolic heat conduction equation are used to study the laser-surface interactions whose time periods are on the order of the material thermal relaxation time (Qiu and Tien, 1992; Vedavarz et al., 1994). If the thermal relaxation time is much smaller than the pulse width, the Fourier heat conduction equation should be applicable (Joseph and Preziosi, 1989). The thermal relaxation time τ_h can be expressed as $\tau_h = 3\alpha/\upsilon^2$ from kinetic theory, where $\alpha = k/\rho c_p$ is the thermal diffusivity and υ is the speed of sound in the medium (Honner and Kunes, 1999).

In the present study, the pulse width is on the order of nanoseconds and the speeds of sound in glass and copper are taken as υ = 5640, 5010 m/s, respectively (Weast et al., 1981). The thermal diffusivities of the glass and copper are 4.53×10^{-7} m^2/s and

1.17×10^{-4} m^2/s, respectively. The thermal relaxation times of glass and copper determined by the above equation are on the orders of 10 fs and 10 ps, respectively. Their thermal relaxation times are much smaller than the laser pulse width. Hence, the Fourier's heat conduction equation is appropriate for studying the thermal response of glass and copper under the heating of laser pulse on the order of nanoseconds.

The transient response of the volume-absorbing glass to the incident laser pulse can be described by the three-dimensional heat conduction equation with internal heat generation:

$$\nabla^2 T_g + \frac{\dot{q}(x,y,z,t)}{k_g} = \frac{1}{\alpha_g}\frac{\partial T_g}{\partial t} \tag{3-17}$$

The transient response of the copper is described by the heat conduction equation without heat generation:

$$\nabla^2 T_c = \frac{1}{\alpha_c}\frac{\partial T_c}{\partial t} \tag{3-18}$$

In Eqs. (3-17) and (3-18), T_g and T_c are the temperatures of the glass and copper, α_g and α_c are the thermal diffusivities of the glass and copper, respectively; k_g is the thermal conductivity of glass and $\dot{q}(x,y,z,t)$ is the total heat generation rate. The initial and boundary conditions are discussed in the respective modeling in subsequent chapters.

Finite Element Method

A commercial finite element software package, ANSYS, is employed to model the thermal responses of glass and copper to the different heating processes. Several finite element models are built using ANSYS 5.4-5.6. In the finite element system, the Fourier's heat conduction equation can be expressed as (Kohnke, 1997)

$$[\mathbf{C}]\{\dot{\mathbf{T}}\}+[\mathbf{K}]\{\mathbf{T}\}=\{\dot{\mathbf{Q}}\} \tag{3-19}$$

where $\mathbf{C}$ and $\mathbf{K}$ are the heat capacity and thermal conductivity matrices, $\mathbf{T}$ and $\dot{\mathbf{T}}$ are the nodal temperature and its time derivative vectors, respectively; $\dot{\mathbf{Q}}$ is the effective heat flow vector including the heat generation rate, the convection and radiation heat flows. The radiation part $\dot{\mathbf{Q}}_{\mathbf{r}}$ of the effective heat flow $\dot{\mathbf{Q}}$ can be written as

$$\{\dot{\mathbf{Q}}_{\mathbf{r}}\}=[\mathbf{K}']\{\mathbf{T}\} \tag{3-20}$$

where $\mathbf{K}'$ is the radiation matrix determined by the view factors and $\mathbf{T}^3$ terms. In the finite element model, different elements are used for applying the heat generation rate, the convection and radiation heat flows.

The solution method employed for Eq. (3-19) is the generalized trapezoidal rule, in which a transient integration parameter is introduced. The Crank-Nicholson method is used for the transient integration parameter of 0.5 and the backward Euler method is used for the transient integration parameter of 1. When the transient integration parameter is equal or greater than 0.5, the solution for these equations is unconditionally stable. The generalized-trapezoidal method requires that the initial conditions must be input prior to the start of the transient analysis.

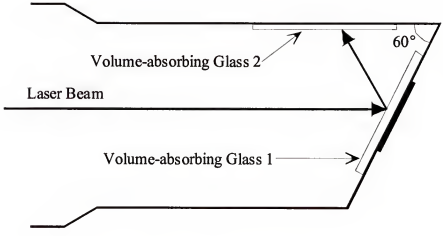

Figure 3-1. Schematic of the cavity in 193-nm calorimeter.

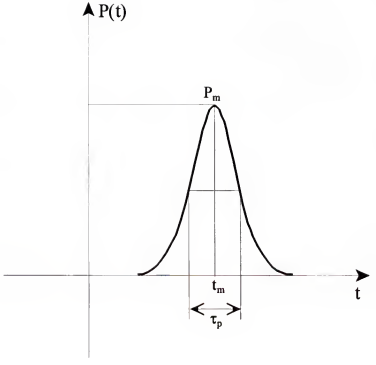

Figure 3-2. Gaussian distribution of laser power with time.

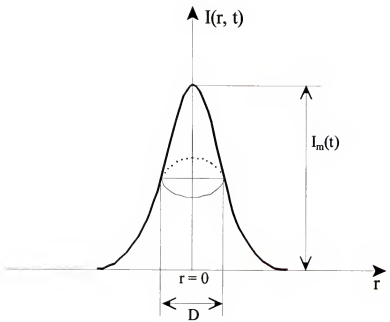

Figure 3-3. Gaussian distribution of laser intensity with space.

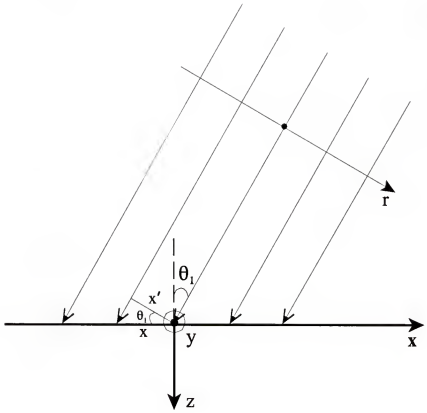

Figure 3-4. Schematic of the tilted laser incidence.

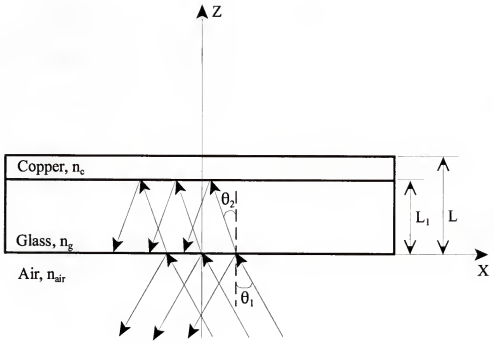

Figure 3-5. Illustration of the thermal model.

CHAPTER 4
ANALYSIS OF THERMAL MECHANISMS IN VOLUME ABSORBER

This chapter presents the thermal modeling and analysis of the volume absorber based on the design of the pulsed excimer laser calorimeters at the wavelength of 193 nm. In this work, Gaussian distributions are used to model the temporal and spatial distributions of the laser beam for simplifying the modeling method and the Beer-Lambert law is used to model the internal absorption of the laser power; the absorption of laser energy in the volume-absorbing glass is described by the heat generation rate derived in Chapter 3. A finite element method is employed to simulate the space- and time-dependence of temperature in the volume absorber. A three-dimensional model is used to study the heating effects of single pulse and an axisymmetric model is built for modeling the multiple-pulse heating process. The fundamental thermal mechanisms of pulsed-laser heating on the volume-absorbing material is analyzed based on the modeling results.

Thermal Model of the 193 nm Calorimeter

Design of the 193 nm Calorimeter

Based on the work of Leonhardt and Scott (1995) of the 248-nm laser calorimeter, a design was made for the 193 nm calorimeter as shown in Fig. 4-1. The calorimeter cavity made of thin copper is suspended in an isothermal heat sink. An electrical heater is attached to the back of the bottom plate to calibrate the calorimeter

electrically. Two volume-absorbing glass plates for absorbing the energy of excimer laser are epoxied to the inside walls of the cavity. The glass plates are used to absorb the radiant energy during laser heating and the absorbed energy is transferred from glass to copper through heat conduction and to the surrounding volume through convection and radiation. During electrical heating process, the energy provided by the electrical heater quickly diffuses to other parts of the cavity and the glass plate, which is then transferred to the surrounding through convection and radiation. Another heat flow path is the conduction of heat from the calorimeter cavity to the isothermal heat sink through the supports which mount the cavity to the heat sink. The calibration factor, which links the thermal response to the absorbed optical energy, is determined from the electrical heating process.

In order to select the volume-absorbing glass appropriate for the excimer laser at the wavelength of 193 nm, thermal modeling and analysis are performed to obtain the temperature distribution of the glass and copper at the bottom of the cavity, during and after the pulse heating. The effects of various pulse parameters on the maximum temperature rise are examined. Although the thermal time constant of the calorimeters is on the order of 10 s, understanding the heat transfer mechanisms in the bottom plate of the cavity during short (nanoseconds) pulse hearting is very important for the design and evaluation of 193 nm pulsed-laser calorimeters.

Thermal Model of the Volume Absorber

This study is focused on the volume-absorbing glass at the back of the absorbing cavity and the copper plate attached to the glass. The schematic of thermal model used in

this modeling is shown in Fig. 3-5. In the present study, the thickness of the copper plate is 0.2 mm; the volume-absorbing glass at the back of cavity is a square plate with a thickness 0.1 cm and an area $3.2\,\text{cm} \times 3.2\,\text{cm}$ and its absorption coefficient is 63 cm^{-1}. The laser beam is incident on the glass surface at an angle $\theta_1 = 30°$. The reflectance R_g of glass surface depends on the refractive index of the glass, the angle of incidence and the polarization of laser beam (Siegel and Howell, 1992). The reflectance can be determined using the Fresnel reflection coefficients:

$$\tilde{r}_{12} = \frac{n_1 \cos\theta_1 - \tilde{n}_2 \cos\theta_2}{n_1 \cos\theta_1 + \tilde{n}_2 \cos\theta_2} \qquad \text{for s-polarization} \tag{4-1}$$

$$\tilde{r}_{12} = \frac{n_1 \cos\theta_2 - \tilde{n}_2 \cos\theta_1}{n_1 \cos\theta_2 + \tilde{n}_2 \cos\theta_1} \qquad \text{for p-polarization} \tag{4-2}$$

In Eqs. (4-1) and (4-2), $\tilde{r}_{12}$ is the complex Fresnel's reflection coefficient; $n_1 = 1$ is the refractive index of air; $\tilde{n}_2 = n_2 + i\kappa_2$ is the complex refractive index of the crystal; and θ_2 is an angle determined by Snell's law:

$$n_1 \sin\theta_1 = \tilde{n}_2 \sin\theta_2 \tag{4-3}.$$

The reflectance R at the interface between air and the crystal is $R = |\tilde{r}_{12}|^2$ for s-polarized or p-polarized laser beam. The reflectance for non-polarized laser beam is the average of the reflectance for s-polarization and p-polarization. In the present study, the laser beam is considered as non-polarized beam and the reflectance R_g is determined as 0.041 by using the optical properties of glass listed in Table 4-1.

In this thermal model, the repetition rate of laser pulse is 50 Hz, the energy of one pulse is 5 J, the FWHM pulse width is 30 ns, the FWHM beam diameter is 1 cm, and the glass is assumed not to be damaged. The volume-absorbing glass is optically thick

because of the thickness of 0.1 cm and the absorption coefficient of 63 cm^{-1}. The laser intensity at the interface between glass and copper is 0.18% of the transmitted intensity at the glass surface, indicating almost the total transmitted energy is absorbed in the glass. Hence, the heat flux caused by the incident laser on the copper surface and the reflected energy are neglected. The heat generation rate in glass caused by the absorption of the transmitted laser at the glass surface is given by Eq. (3-11).

The front surface of glass and the back surface of copper are subjected to convection and radiation boundary conditions as the following:

$$k_g \left.\frac{\partial T_g}{\partial z}\right|_{z=0} = h_g[T_g(x,y,0,t) - T_0] + \varepsilon_g \sigma[T_g^4(x,y,0,t) - T_0^4] \tag{4-4}$$

$$-k_c \left.\frac{\partial T_c}{\partial z}\right|_{z=L} = h_c[T_c(x,y,L,t) - T_0] + \varepsilon_c \sigma[T_c^4(x,y,L,t) - T_0^4] \tag{4-5}$$

The total emissivities of glass surface and copper surface are shown in Table 4-1. Even though the natural convection coefficient is temperature dependent, a constant convection coefficient of 8 $W/m^2 \cdot K$ is used in the current model. The side surfaces of the glass and copper are considered isothermal because the single-pulse heating has very little influence on the temperature field away from the center. Notice that the temperatures at the side surfaces of the glass and copper are set to ambient temperature T_0. The boundary conditions at the interface between the absorbing glass and the copper are

$$T_g(x,y,L_1,t) = T_c(x,y,L_1,t) \tag{4-6}$$

$$k_g \left.\frac{\partial T_g}{\partial z}\right|_{z=L_1} = k_c \left.\frac{\partial T_c}{\partial z}\right|_{z=L_1} \tag{4-7}$$

The initial condition of glass and copper are set to the ambient temperature T_0:

$$T_g(x,y,z,0) = T_c(x,y,z,0) = T_0 \tag{4-8}$$

In the modeling, the ambient temperature T_0 is set to 300 K.

Three-Dimensional Modeling

Three-Dimensional Model

A three-dimensional model is built using finite element software Ansys 5.4, which is based on the thermal model of the volume absorber. Although the Gaussian distribution extends from $-\infty$ to $+\infty$, it decreases quickly away from the peak. In the present study, the heat generation rate is computed for $r \le 2D$ and from $t_m - 2\tau_p$ to $t_m + 2\tau_p$, and it is set to be zero otherwise. Because the laser beam is inclined only in x direction, the temperature distribution of the absorbing glass and copper is symmetric about the x-z plane. Only half of the glass and copper plates ($y \ge 0$) is studied.

The thermophysical properties of the glass and copper are assumed constant in the present study and are listed in Table 4-1. The thermophysical properties of copper are obtained from Incropera and DeWitt (1996); the thermophysical properties of glass are provided by Marla Dowell of NIST; the emissivity of glass is referenced from Touloukian and Dewitt (1972) and the optical constants of copper and glass are referenced from Palik (1985). Solid elements are used to model the glass and copper plates, and surface elements are used to model the free convection and radiation boundary conditions. According to the spatial distribution of the heat generation rate and the

numerical test results, the element size in the x-y plane is changed from 0.02 cm close to the center to 0.2 cm near the side boundaries. The mesh scheme in the x-y plane is shown in Fig. 4-2. Three different sizes are used to mesh the glass in the z direction. The element size is 0.001 cm for $0 \le z \le 0.016\,\text{cm}$, 0.003 cm for $0.016\,\text{cm} \le z \le 0.04\,\text{cm}$, and 0.015 cm for $0.04\,\text{cm} \le z \le 0.1\,\text{cm}$. The element size is 0.02 cm in the copper ($0.1\,\text{cm} \le z \le 0.12\,\text{cm}$), i.e., there is only one layer of element in the z direction inside the copper. Calculations show that the maximum temperature increases by 1.6% when the smallest element size in the z direction is reduced from 10 μm to 5 μm. The temperature difference is small enough for the numerical solution to be considered stable, suggesting that the mesh scheme is appropriate.

The initial condition is a uniform temperature T_0 = 300 K inside the glass and copper. The total time required to model one pulse is determined by the inverse of the pulse repetition rate (1/N). For each pulse, the heat generation rate is nonzero only at the initial period equal to $4\tau_p$, i.e., the heating process is from $t_m - 2\tau_p$ to $t_m + 2\tau_p$. For the mth pulse, $t_m = 2\tau_p + (m-1)/N$. In the heating process, the time step size is taken as $\tau_p/5$. The cooling process (without heat generation) is from $t_m + 2\tau_p$ to the beginning of the next pulse, in which the time step size is increased with time from a few nanoseconds to tenths of a second.

Validation of Numerical Modeling

The three-dimensional model can be tested through performing an adiabatic modeling, in which the convection and radiation boundary conditions are closed. The

uniform temperature rise of the adiabatic solid model can be calculated using the following equation:

$$\Delta T = \frac{(1 - R_g) \cdot E}{(mc_p)_g + (mc_p)_c} \tag{4-9}$$

where ΔT is the temperature rise at the steady state, E is the total input energy, R_g is the reflectance of the glass surface, and $(mc_p)_g$ and $(mc_p)_c$ are the heat capacities of glass and copper, respectively. In the three-dimensional solid model, the heat capacities of glass and copper are 1.649 J/K and 0.704 J/K, respectively. When glass is heated using a single pulse with pulse energy of 5 J, the uniform temperature calculated from Eq. (4-9) is 2.04 K and the uniform temperature predicted using the adiabatic three-dimensional model is 2.07 K, which relative error is less than 1.5%.

The validation of element size and time step can be further tested using temperature analysis at the center. When the glass is heated by a single pulse with τ_p = 30 ns, the thermal diffusion length in the $4\tau_p$ heating process can be estimated by $\sqrt{4\tau_p \alpha_g} \approx 0.1$ μm. Hence, heat conduction can be neglected during the heating process. When the surface temperature of the glass is assumed to be 1000 K, the heat loss by free convection is $\approx 10^{-7}$ J/cm^2 and that by radiation is $\approx 10^{-6}$ J/cm^2, which are much less than the laser energy flux at the center of the glass surface. Therefore, the heating process is nearly adiabatic. The adiabatic model is then used to estimate the maximum temperature rise at the end of the heating process. The maximum temperature rise is at the center of the glass surface and can be calculated by the following equation:

$$\Delta T_g = \frac{1}{(\rho c_p)_g} \int_{t_m - 2\tau_p}^{t_m + 2\tau_p} \dot{q}_i(0, 0, 0, t)\, dt \tag{4-10}$$

For the absorption coefficient $a = 63\,cm^{-1}$, pulse width τ_p = 30 ns, and pulse energy Q = 5 J, the maximum temperature rise at the end of the heating process is 152.8 K calculated from Eq. (4-10) and 147 K obtained from the numerical simulation. The relative temperature difference is 3.8%. This difference is mainly caused by the element size in the z direction. When the element size in the z direction is reduced, the numerical result becomes closer to the theoretical prediction. For example, when the element size in the z direction is reduced to 0.1 μm, the temperature rise is 151.8 K and the relative temperature difference is only 0.7%. It takes much more computational time and disk space to model such small elements. Because the objective of the present study is to understand the heat transfer process, extremely high accuracy is not needed. When the time steps are varied in the simulation, it has been found that the step size has little influence on the temperature rise at the end of heating process, presumably because the heating generation rate is symmetric about t_m.

Results and Discussion

The three-dimensional model is used to predict the temperature distributions and histories of the glass and copper heated by a single laser pulse, whose energy is 5 J, FWHM pulse width is 30 ns, and FWHM beam diameter is 1.0 cm. Pulse energy of 5 J is close to the practical limit for most applications of 193 nm lasers. The angle of incidence of the laser beam is 30°. In the three-dimensional model, the influence of the incidence angle on the temperature distribution is considered.

The temperature rises on the glass surface (z = 0) at the end of the heating process are shown in Fig. 4-3. The maximum temperature rise is 147 K at the center of the glass

surface. The diameter of the area with temperature rise from 130.6 to 147 K is about 0.4 cm, indicating the central area with high temperature rises is much smaller than the FWHM cross-sectional area of the laser beam. As a result of the oblique incidence, the heat generation rate inside the glass is not axisymmetric. Influenced by the heat conduction between the surface and the inside, the temperature distribution is not symmetric on the glass surface. When the laser pulse is directly incident on the surface of copper, the maximum temperature rise is calculated to be 4500 K because of the small radiation penetration depth. The maximum temperature rise for a surface absorbing glass would be 2.2×10^5 K for the same pulse parameters. This indicates that the volume absorbing glass is essential for laser calorimeters with short pulses.

The heat generation rate and the temperature history at the center of the glass surface in the heating process are shown in Fig. 4-4. The temperature at the center of the glass surface increases slowly at the beginning and rapidly as $\dot{q}_1$ increases. After 100 ns, the temperature changes little because the heat generation rate is small and the heat loss increases as the temperature rises. When the energy supplied to the center point by laser heating is less than the energy losses caused by the radiation, convection, and the inside conduction, the temperature of the center point of the glass surface goes down. This can be seen clearly in Fig. 4-5, where the temperature histories on the glass surface ($z = 0$) and along the z-axis are shown. In the cooling process, the temperatures on the glass surface decrease, but the temperatures inside the glass increase slightly because the heat gained from the glass surface is more than that transferred towards the copper. The maximum temperature rise at the center of the glass-copper interface (0,0,0.1) is ≈0.13 K, which is very small compared to the 147 K temperature rise at the glass surface. In the

cooling process, the temperature difference at locations (0,0,0.1) and (0,0,0.12) is much less than 1 mK because the thermal conductivity of copper is much greater than that of glass. Compared with the temperature difference in the glass, the copper plate can be regarded as an isothermal layer in the heating process of single pulse.

The effects of laser pulse energy, pulse width, and beam diameter on the maximum temperature rise have been investigated using the finite element model. The maximum temperature rise is proportional to the pulse energy Q. When the pulse width increases from 10 ns to 300 ns, the maximum temperature rise decreases by less than 0.02%. The effects of the pulse energy and pulse width on the maximum temperature rise can be understood from the adiabatic model, i.e., Eq. (4-10). As the beam diameter D increases, the maximum temperature rise decreases by a factor of D^2. This is because $\dot{q}_1$ at the center of glass surface is proportional to the inverse of D^2, see Eqs. (3-11) and (3-12).

Axisymmetric Modeling

Axisymmetric Model

It takes about 5 hours to obtain the temperature distribution of the glass and copper for one pulse using the three-dimensional model, and it needs about 450 Mb disk space to save the database. In order to reduce the computational time and the disk space, an axisymmetric model is developed to simulate the multiple-pulse heating process.

The square glass and copper are simplified to the circular disks with a radius of 1.6 cm and the laser beam is incident on the glass surface perpendicularly, whose incident angle and refractive angle are zeros. The heat generation rate $\dot{q}_1(r,z,t)$ under the normal

incidence of laser beam is determined from Eqs. (3-11) and (3-12) by setting θ_1 and θ_2 to zeros. Notice the reflectance R_g in the Eq. (3-12) is determined under the condition of the normal incidence.

For comparison, the temperature history is also studied when the glass is heated continuously by the average power using the axisymmetric model. The average power is calculated by $P_a = Q \cdot f$ and the spatial distribution of the power is also Gaussian distribution. In the axisymmetric model, the heat generation rate $\dot{q}_1(r,z,t)$ caused by the average power can be derived from Eqs. (3-11) and (3-12) by using Eq. (3-4) under conditions of θ_1 and θ_2 equal to zeros.

In the axisymmetric model, the element sizes in the z direction are the same as those in the three-dimensional model and the element size in the r direction is from 0.02 to 0.1 cm. The axisymmetric model is also tested through performing the adiabatic modeling for pulse heating and average-power heating. The uniform temperature rise of the adiabatic circular plates of glass and copper is 2.60 K calculated from Eq. (4-9) when the glass is heated by a single pulse with pulse energy of 5 J. The temperature rise at the steady state for pulse heating and average-power heating are 2.62 K and 2.63 K predicted by the axisymmetric model, respectively. The relative errors for pulse heating and average-power heating are less than 1.2%. The peak temperature in the first pulse heating is calculated as 165.8 K by substituting $\dot{q}_1(0,0,t)$ for multiple-pulse heating in-to Eq. (4-10). This peak temperature predicted from axisymmetric model is 160.7 K, which relative error is less than 3.1%. It is unnecessary to pursue higher accuracy by reducing the element size significantly. Hence, the current element sizes and time steps are employed for modeling the pulsed-laser heating and average-power laser heating.

Results and Discussion

The multiple-pulse heating is studied using the axisymmetric model with pulse heating and average-power heating. Figs. 4-6 and 4-7 show the temperature rises at (0,0,0) and (0,0,0.1) during the first ten pulses with a pulse energy Q = 5 J, width τ_p = 30 ns, repetition rate f = 50 Hz, and beam diameter D = 1.0 cm, together with those for continuous heating with an average power P_a = 250 W. Notice that the temperature at the back surface of copper (0,0,0.12) is very close to that at (0,0,0.1). For the pulse heating, the temperature at the center of the glass surface goes up quickly in the heating process of each pulse, drops suddenly at the beginning of the cooling process, and then goes down slowly until the next pulse. The temperature at (0,0,0) goes up gradually for continuous heating. The maximum temperature must not exceed the damage threshold, which limits the number of pulses that can be measured by the calorimeter. Because the peak temperature is much higher for the pulse heating than for the average-power heating at the first several pulses, the heat loss at the glass surface is greater for pulse heating in the initial period. As shown in Fig. 4-6, the difference between the maximum temperature rise for pulse heating and that for average-power heating becomes smaller with increase of the pulse number. As seen from the Fig. 4-7, the temperature of the back surface for multiple-pulse heating is higher than that in the average-power heating because the heat conduction inside the glass is faster for pulse heating than for continuous heating.

The maximum temperature rise in the first pulse heating predicted by the axisymmetric model (at normal incidence) is 161 K which is higher than that predicted by the three-dimensional model with laser beam incidence at θ_1 = 30°. Although the effective path length is longer for oblique incidence than for normal incidence, less

energy is absorbed at the center of glass surface due to the decrease of energy flux on the surface with the increase of θ_1. (The effective path length is $z/\cos\theta_2$.) This can also be explained by Eq. (3-12) that the heat generation rate at the center of the glass surface is proportional to $\cos\theta_1$. Notice that the reflectance is almost the same for $\theta_1 = 0°$ and $\theta_1 = 30°$. Hence, the absorbed energy causes a lower heat generation rate near the glass surface for tilted incidence, which in turn causes a lower temperature rise at the center of the glass surface.

Analysis of the Proposed Design

A modified design is proposed based on the modeling results of the volume-absorber, in which the volume absorber is not optically thick. Under consideration of the reflection at the interface and the absorption on the copper surface, a one-dimensional model is built for the adiabatic heating process of the single pulse and used to study the influence of the glass absorption coefficient on the maximum temperature at the centers; the axisymmetric model is extended to model the temperature distribution of glass with low absorption coefficient for multiple-pulse heating. The comparison with previous results shows that the energy loss and nonequivalence in the proposed design are smaller. Hence, this proposed design can increase the accuracy and dynamic range of calorimeters. This work will help the future improvement of optical calorimeters for measuring the pulse energy of excimer lasers in the deep ultraviolet.

Modeling of the Proposed Design

For the volume-absorbing glass with absorption coefficient of 63 cm^{-1}, the thickness of the glass is 6.3 times the radiation penetration depth ($\lambda/4\pi\kappa$). When the laser

pulse is incident on the volume-absorbing glass, almost all of the transmitted energy of laser pulse is absorbed inside the glass and there is a negligible surface heating on the copper surface adjoining the glass. The maximum temperature is on the glass surface and the temperature decreases as z increases. It takes a long time to transfer heat from the glass to copper because of the lower thermal conductivity of glass. As a result, the energy loss is larger for pulse heating than for electrical heating, because in the electrical calibration the highest temperature is located on the back surface of copper where the electrical heater is attached. This will decrease the accuracy of the laser calorimeter. The high peak temperature on the glass surface may limit the maximum measurement energy, and hence reduce the dynamic range of the calorimeter. As the absorption coefficient of the glass decreases, part of the laser energy will penetrate through the glass and be absorbed directly by the copper surface. Moreover, some of energy will be reflected by the copper surface, resulting in additional heat generation inside the glass. This should help reduce the maximum temperature on the glass surface and heat losses from the glass surface by convection and radiation during pulsed-laser heating.

In the proposed design with a normal incidence of laser beam, the additional heat generation rate $\dot{q}_2(r,z,t)$ caused by the reflected energy from the copper surface can be derived from Eqs. (3-13) and (3-14), and heat flux $q''(r,L_1,t)$ on the interface can be derived from Eqs. (3-15) and (3-16), by setting θ_1 and θ_2 to zeros. Notice R_c is the reflectance of the copper surface with a value of 0.277.

For the heating time of 120 ns, the thermal diffusive length in the copper is 3.75 μm. Hence, the points beyond 3.75 μm from the center point have little influence on the temperature of the center point. The heat generation rate and heat flux change so little

within a few micrometers from the center point that can be considered uniform. Hence, a one-dimensional model is used to study the temperature change near the center of the laser beam, in which the laser beam is incident normal to the glass surface. In the one-dimensional model, the heat generation rate and the heat flux on the copper surface in the x-y plane are uniform, equal to the values at the center; in the glass, the element size in the z direction is 0.001 cm for $0 \le z \le 0.01\,\text{cm}$, 0.01 cm for $0.01\,\text{cm} \le z \le 0.09\,\text{cm}$, 0.001 cm for $0.09\,\text{cm} \le z \le 0.099\,\text{cm}$ and 0.0001 cm for $0.099\,\text{cm} \le z \le 0.1\,\text{cm}$; in the copper, the element size in the z direction is 0.0001 cm for $0.1\,\text{cm} \le z \le 0.101\,\text{cm}$, 0.001 cm for $0.101\,\text{cm} \le z \le 0.11\,\text{cm}$ and 0.01 cm for $0.11\,\text{cm} \le z \le 0.12\,\text{cm}$. The smaller elements are used around the glass-copper interface for the consideration of the heat flux on the copper surface.

Results and Discussion

The maximum temperature rise on the glass surface and that on the copper surface adjoining the glass are shown in Fig. 4-8 as functions of the absorption coefficient for Q = 5 J, D = 1 cm and τ_p = 30 ns. As the absorption coefficient decreases, the maximum temperature rise on the copper surface increases due to surface heating, whereas the maximum temperature on the glass surface decreases due to the redistribution of the heat generation rate. When the absorption coefficient becomes smaller than 40 cm^{-1}, the maximum temperature rise on the copper surface is higher than that on the glass surface. Under such conditions, heat is transferred to copper rapidly and the energy loss on the glass surface is small. Therefore, the accuracy and dynamic range of the calorimeter can

be improved by selecting an absorbing glass with smaller absorption coefficient or simply reducing the thickness of the glass in the present design.

The temperatures at the centers of the glass surface (0,0,0) and the copper surface (0,0,0.1) in the heating process are shown in Fig. 4-9 for a = 30 cm^{-1}. The temperature of the copper surface increases faster than that of the glass surface because of the surface heating effect. Although the maximum temperature rise on the copper surface of 188.5 K is much higher than that on the glass surface, it drops rapidly because the thermal conductivity of copper is much greater than that of glass. The temperature gradient in the z direction after the heating process is much less in this case than in the previous case with a = 63 cm^{-1}, see Fig. 4-5.

The axisymmetric model has been extended to study the multiple-pulse heating process for absorption coefficients below 63 cm^{-1}. In this model, the heat flux on the copper surface and the additional heat generation rate caused by reflection from the copper surface are considered and the element sizes in the z direction are same as those in the one-dimensional model. This axisymmetric model is also tested using adiabatic analysis. The uniform temperature predicted by the modeling is 2.62 K when glass is heated by a single pulse with pulse energy of 5 J. Compared with the theoretical value 2.60 K calculated from Eq. (4-9), the relative error is less than 1%.

Thermal responses of glass and copper to multiple-pulse heating are predicted using the axisymmetric model for the absorption coefficient of glass a = 30 cm^{-1} and the same pulse parameters as those for Figs. 4-6 and 4-7. Figure 4-10 shows the temperature rises at the centers on the glass surface (z = 0) and copper surface (z = 0.1) during the first five pulses heating. The results of the axisymmetric model and the one-dimensional

model are almost the same in the heating process of the first pulse. After the heating process of the first pulse, however, lateral heat conduction becomes important and the one-dimensional model fails to predict the temperature history at the centerline. In the heating process of each pulse, the temperature at (0,0,0.1) increases and decreases suddenly. Due to the heat conduction from the glass to copper, the temperature at (0,0,0.1) increases slightly in the cooling process of each pulse. Compared to the previous results (see Figs. 4-6 and 4-7), the temperature at the center of the glass surface is much smaller at the end of the heating process of each pulse. For example, at the end of the first pulse and fifth pulse, the temperature rises at (0,0,0) are respectively 78 K and 281 K as shown in Fig. 4-10, which are much smaller than the corresponding values of 161 K and 462 K in Fig. 4-6. Because of the low thermal conductivity of glass, the temperatures on the glass surface do not drop very much in the cooling processes. Consequently, the temperature at (0,0,0) keeps rising as the number of pulse increases. The maximum temperature on the glass surface exceeds that on the copper surface (0,0,0.1) after four pulses. Hence, the damage threshold of glass limits the number of pulses in the multiple-pulse heating process. Further analysis of the proposed design is needed so that the optimized absorption coefficient can be determined.

The epoxy between glass and copper is not considered in the thermal analysis; however, the thermally conducting epoxy between glass and copper may act as an energy absorber. The high temperature predicted for multiple-pulse heating may cause phase transition in the glass; this is not considered in the current model. Because the pulse energy (Q = 5 J) used in this study is much high, the nonlinear effects caused by

multiphoton absorption may be significant. The effect of multiphoton absorption will be discussed in the next chapter.

Table 4-1. Thermophysical properties of the absorbing glass and copper

	Glass	Copper
Thermal Conductivity, k (W/cm·K)	0.0073	4.01
Density, ρ (g/cm^3)	2.3	8.933
Specific Heat, c_p (J/g·K)	0.7	0.385
Total Emissivity, ε	0.8	0.03
Refractive Index, n	1.5	0.958
Extinction Coefficient, κ	9.68×10^{-5}	1.37

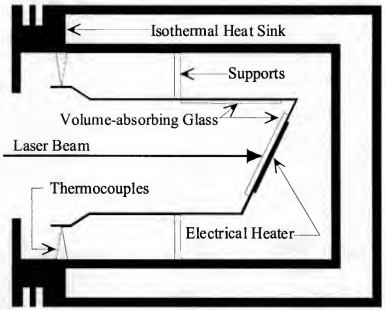

Figure 4-1. Schematic of the 193-nm calorimeter cavity.

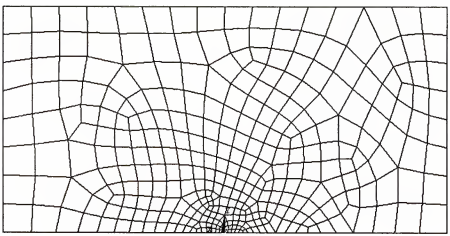

Figure 4-2. Mesh scheme on the x-y plane.

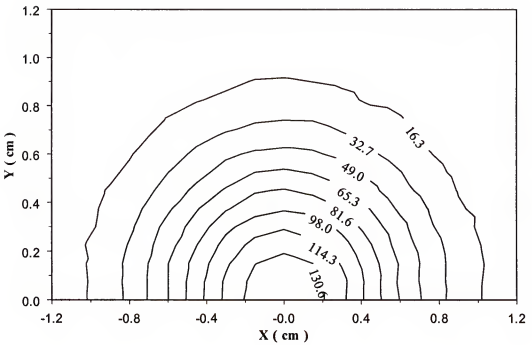

Figure 4-3. Temperature contour of the glass surface at the end of the heating process, showing temperature difference $T - T_0$ in K.

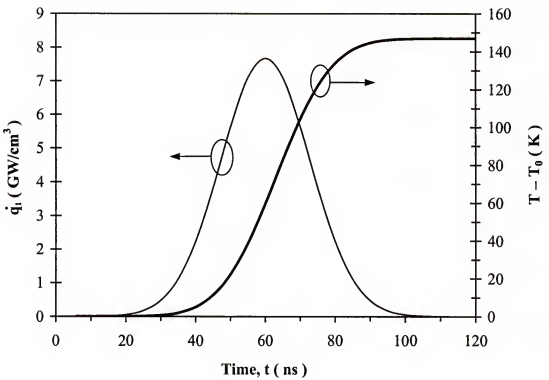

Figure 4-4. Heat generation rate and temperature history at the center point of the glass surface in the heating process.

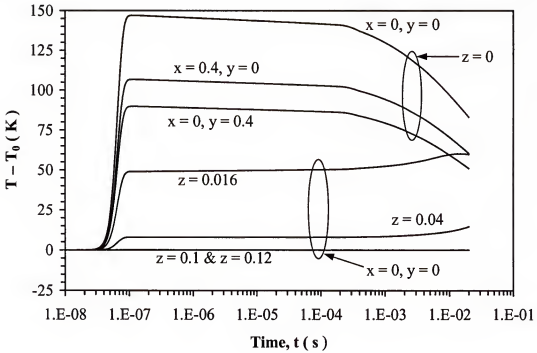

Figure 4-5. Temperature histories on the glass surface (z = 0) and along the z-axis (x = 0, y = 0).

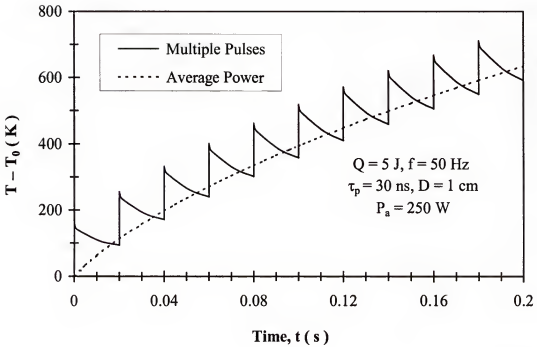

Figure 4-6. Comparison of the temperature histories for multiple-pulse heating and average-power heating at glass surface (0,0,0).

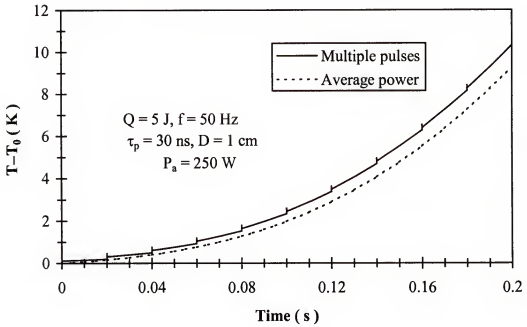

Figure 4-7. Comparison of the temperature histories for multiple-pulse heating and average-power heating at copper surface (0,0,0.1).

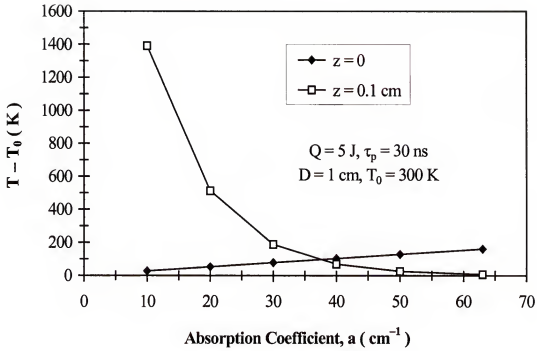

Figure 4-8. Comparison of the maximum temperature rise at z = 0 (glass surface) to that at z = 0.1 cm (copper surface).

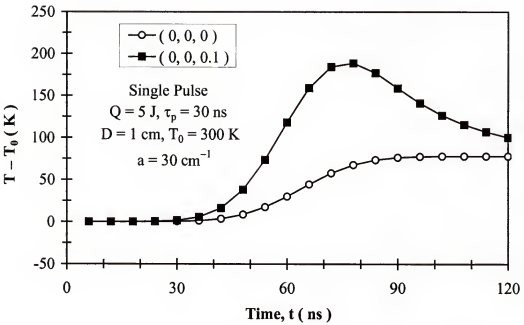

Figure 4-9. Comparison of the temperature history at (0, 0, 0) to that at (0, 0, 0.1) in the heating process of single pulse.

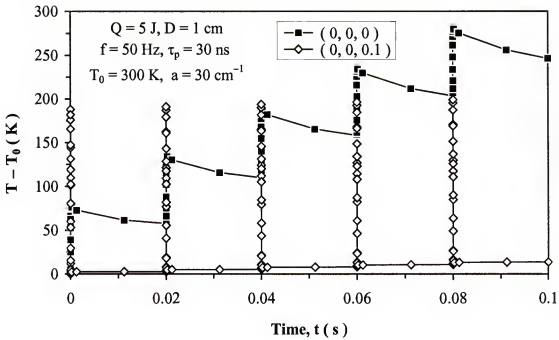

Figure 4-10. Comparison of the temperature history at (0, 0, 0) to that at (0, 0, 0.1) in the heating process of multiple pulses.

CHAPTER 5
MULTIPHOTON ABSORPTION IN VOLUME-ABSORBING GLASS

Two-photon absorption in volume-absorbing materials may be significant for high-power, short-pulse excimer laser irradiation. In this chapter, the laser intensity in ultraviolet (UV) absorbing glass with one- and two-photon absorption is derived, and the effects of two-photon absorption on the intensity propagation and the penetration depth are investigated. The temperature histories for single- and multiple-pulse heating are predicted using an axisymmetric model with one- and two-photon absorption. The heat generation rate caused by one- and two-photon absorption is determined for pulsed laser heating with Gaussian distributions in both space and time. The results show that the two-photon absorption can compress the volume-absorbing effect to surface absorption and increase the peak temperature on the glass surface. This will reduce the damage threshold, increase the energy loss, and reduce the accuracy of pulsed-laser calorimeters. It is expected that a better understanding of the thermal response of the volume-absorbing materials under excimer laser irradiation will yield improvements in the future design of pulsed-laser calorimeters.

Introduction

In the previous chapters, the thermal responses of volume-absorbing glass under single- and multiple-pulse heating have been studied; the temperature history and

distribution were predicted and compared with those under continuous-wave laser heating; furthermore, the influence of the glass absorption coefficient on the absorbed laser energy distribution was also investigated. However, the nonlinear behavior due to multiphoton absorption was not considered, which may be significant at high laser intensities. Multiphoton absorption has been studied by many researchers in recent years along with the development of high-power, short-pulse lasers. Taylor et al. (1988) measured the two-photon absorption coefficient at 248 nm wavelength for a number of window materials including fused silica and CaF_2. Longtin and Tien (1997) investigated the mechanisms of multiphoton absorption in liquids and developed a thermal model from microscopic considerations. Kittlemann and Ringling (1994) measured the intensity-dependent transmission properties and two-photon absorption coefficients of window materials for 193 nm excimer laser irradiation. Brimacombe et al. (1989) measured the two-photon absorption coefficient of fused silica fibers at several excimer laser wavelengths. The two-photon absorption at 193 nm has been shown to cause color center formation (additional absorption) and densification (change in optical path length) in synthetic fused silica (Seward III et al., 1997; Mann and Eva, 1998). Under the irradiation of 193 nm excimer lasers with high pulse energy and short pulse duration, the two-photon absorption in the UV-absorbing glass may significantly influence the thermal behavior of the pulsed-laser calorimeters.

Laser Intensity and Penetration Depth

The single-photon and two-photon absorption mechanisms are shown schematically in Fig. 5-1. It is assumed that the single-photon absorption is due to the

trap-site ionization and the two-photon absorption excites electrons from the valence band to the conduction band (Taylor et al., 1988; Weitzman and Osterberg, 1996). The probability of multiphoton absorption increases with the photon energy, which is determined by the laser wavelength. The band gap of fused silica is on the order of 10 eV (Weitzman and Osterberg, 1996), while the photon energy is 6.4 eV at the wavelength of 193 nm. Hence, two-photon absorption can exist in the volume-absorbing glass under 193 nm excimer laser irradiation. Because two-photon absorption is intensity dependent, it becomes significant in the volume-absorbing glass for high-power, short-pulse irradiation.

The thermal model of the volume-absorbing glass and copper disks involved in this study is shown in Fig. 5-2. The radius of the glass and copper is 1.6 cm, the thickness of the glass is 0.1 cm, and the thickness of the copper is 0.02 cm. The laser beam is incident on the glass surface normally, and most of the laser energy is transmitted into the glass and absorbed inside the glass. In the volume-absorbing glass, the laser intensity attenuation in the direction of propagation (z direction) due to one- and two-photon absorption is governed by the following equation (Weitzman and Osterberg, 1996)

$$\frac{dI}{dz} = -aI - \beta I^2 \tag{5-1}$$

where I is the laser intensity, a is the one-photon absorption coefficient, and β is the two-photon absorption coefficient. In Eq. (5-1), it is assumed that the glass is optically thick (opaque) to the incident radiation (an assumption that will be justified later). By integrating Eq. (5-1), the laser intensity distribution in the z direction is obtained as (Zhang and Chen, 2001)

$$I(z) = \frac{aI_0 e^{-az}}{a + \beta I_0 (1 - e^{-az})} \tag{5-2}$$

where I_0 is the transmitted intensity at the incident surface. For the glass material with a refractive index of approximately 1.5, the reflectivity of glass is calculated to be 0.04, indicating that the transmitted intensity is 96% of the incident intensity at the glass surface.

The penetration depth δ is defined as the distance z at which $I(z)/I_0$ is equal to 1/e. For one-photon absorption, the penetration depth is equal to 1/a and is independent of the laser intensity. When the laser beam is subject to one- and two-photon absorption, the penetration depth is derived from Eq. (5-2) as

$$\delta = \frac{1}{a} \ln\left(\frac{e + \beta I_0 / a}{1 + \beta I_0 / a}\right) \tag{5-3}$$

The penetration depth will decrease as the one-photon and two-photon absorption coefficients increase.

In the present study, the value of a = 63 cm^{-1} is used for the one-photon absorption coefficient of the glass material. Without the two-photon absorption, the internal transmittance is less than 0.2%; hence the optically thick assumption required for Eq. (5-1) is appropriate. Brimacombe et al. (1989) measured two-photon absorption coefficients of glass fibers and obtained $\beta = 1.8 \times 10^{-9}$ cm/W for $a = 5.4 \times 10^{-3}$ cm^{-1}. The one-photon absorption coefficient of the glass used in the present study is 4 orders of magnitude greater than that for the glass fibers studied in (Brimacombe et al., 1989). The two-photon absorption coefficient could increase by the same orders of magnitude as the one-photon absorption coefficient. Because data on the two-photon absorption coefficient for the UV-absorbing glass is not available, in the present study, the effect of

the two-photon absorption is investigated by varying β from 0 to 10^{-5} cm/W. Figure 5-3 shows the intensity distribution calculated from Eq. (5-2) in the 0.1 cm thick glass with $I_0 = 10^9$ W/cm^2. If there is only one-photon absorption ($\beta = 0$), the laser intensity decays exponentially. It can be seen from Eqs. (5-1) and (5-2) that the two-photon absorption will not be so important when $\beta I_0 / a << 1$. For $\beta = 10^{-8}$ cm/W, ($\beta I_0 / a = 0.16$), the intensity distribution deviates slightly from the exponential decay. Further increase of the two-photon absorption coefficient causes the intensity to decay much faster and the distribution to deviate significantly from the single exponential function. When $\beta = 10^{-5}$ cm/W, $\beta I_0 / a = 160$ and hence the absorption process is dominated by two-photon absorption. For $\beta = 10^{-5}$ cm/W about 90% of the laser energy is absorbed within a 10 μm thickness; whereas for $\beta = 0$ only 10% of the laser energy is absorbed within the same thickness. Therefore, the volume-absorbing effect is compressed to surface absorption when two-photon absorption dominates.

The penetration depth is reduced with two-photon absorption. Figure 5-4 shows the ratio of the penetration depth considering two-photon absorption calculated from Eq. (5-3) to $\delta_0 = 1/a$ (without two-phonon absorption), as a function of the dimensionless parameter $\beta I_0 / a$. The penetration depth decreases rapidly as ($\beta I_0 / a$) increases. The normalized penetration depth δ / δ_0 becomes 0.1 for $\beta I_0 / a$ = 15 and 0.02 for $\beta I_0 / a$ = 84. The penetration depth is plotted as a function of the laser intensity for different β values, as shown in Fig. 5-5, with the same one-photon absorption as in Fig. 5-3. At high laser intensity, the penetration depth can be significantly reduced with two-photon absorption. For relatively low two-photon absorption coefficients ($\beta < 10^{-8}$ cm/W), the

penetration depth decreases slightly with increasing laser intensity. For high two-photon absorption coefficients, the penetration depth decreases rapidly as the laser intensity increases. When $\beta = 10^{-5}$ cm/W, the penetration depth drops from 159 μm ($I_0 = 0$) to 2 μm at $I_0 = 10^9$ W/cm^2 and to 0.2 μm at $I_0 = 10^{10}$ W/cm^2. Hence, the volume-absorbing effect can be compressed to surface absorption with two-photon absorption at sufficiently high laser intensities.

The Axisymmetric Heating Model

A finite element model has been developed to study the temperature distribution in the laser calorimeter (see Fig. 5-2). In this model, it is assumed that the laser intensity follows Gaussian distributions in both time and space. Hence, the transmitted intensity I_0 at the incident glass surface ($z = 0$) can be expressed as

$$I_0(r,t) = \frac{(1-R_g)Q}{\pi^{3/2}b^2\tau} e^{-r^2/b^2} e^{-(t-t_m)^2/\tau^2} \tag{5-4}$$

where R_g is the reflectance at the glass surface ($R_g = 0.04$), Q is the energy per pulse, t_m is the time at which the power is maximum, b is related to the full width at half maximum (FWHM) beam diameter D by $D = 2b\sqrt{\ln 2}$, and τ is related to the FWHM pulse width by $\tau_p = 2\tau\sqrt{\ln 2}$.

When the laser beam propagates in the volume-absorbing glass, its energy is absorbed due to the one- and two-photon absorption. The absorbed laser energy is treated as an internal heat generation source in the thermal modeling, and hence,

$$\dot{q}_1(r,z,t) = \frac{a^2 I_0 (a+\beta I_0) e^{-az}}{[a+\beta I_0(1-e^{-az})]^2} \tag{5-5}$$

where $I_0 = I_0(r,t)$ given in Eq. (5-4). Although the Gaussian distribution extends from $-\infty$ to $+\infty$, it decreases quickly away from the peak. In the two-dimensional modeling, the heat generation rate is computed for $r \le 2D$ and from $t_m - 2\tau_p$ to $t_m + 2\tau_p$, and it is set to be zero otherwise. The spatial distribution for a typical 193 nm excimer laser is Gaussian in one direction and uniform in the other direction. In the present study, however, an axisymmetric Gaussian distribution is used to simplify the modeling.

In the heating model, the thermal conductivity, density, and specific heat of the glass are taken from Table 4-1 as k = 0.73 W/m·K, ρ = 2300 kg/m^3, and c_p = 700 J/kg·K, respectively. The copper plate attached to the volume-absorbing glass is also involved in the two-dimensional modeling without considering the thermal contact resistance. The thermal conductivity, density, and specific heat of copper are k = 401 W/m·K, ρ = 8933 kg/m^3 and c_p = 385 J/kg·K from Table 4-1, respectively. In the modeling, thermal properties of the glass and copper are treated as constants for the sake of simplicity. The Fourier's heat conduction equations are solved using the heat generation rate given by Eq. (5-5). The convection and radiation conditions are modeled using a convection coefficient of 8 W/m^2·K and emissivity of 0.8 for the glass surface and 0.01 for the gold-coated copper surface, which are same as those in Chapter 4. The initial temperature of the glass and copper is equal to the ambient temperature T_0, which is set as 300 K. The time at peak power for the mth pulse is $t_m = 2\tau_p + (m-1)/f$, where f is the repetition rate (number of pulses per second). The temperature distribution and history are modeled at different two-photon absorption coefficients (β = 0, 10^{-7}, and 10^{-6} cm/W) with the one-photon absorption coefficient fixed at 63 cm^{-1}.

The element sizes and time steps are carefully selected and tested for numerical convergence. For the glass, the element size in the z direction increases from 2 μm at the glass surface ($z = 0$) to 100 μm at the interface ($z = 0.1$ cm). For the copper, there is only one layer of elements with a thickness of 0.02 cm. Because the process during a single-pulse laser heating (120 ns) is essentially adiabatic, the peak temperature rise ΔT_g at the center of the glass surface can simply be evaluated by the use of the following equation:

$$\Delta T_g = \frac{1}{(\rho c_p)_g} \int_{t_m-2\tau_p}^{t_m+2\tau_p} \dot{q}_1(0, 0, t)\, dt \tag{5-6}$$

After the single-pulse heating (with a laser pulse width $\tau_p = 15$ ns, beam diameter D = 0.5 cm, and pulse energy Q = 1 J), the peak temperature predicted by the finite element model is 0.9%, 1.2%, and 4.4% lower than those calculated from Eq. (5-6) for $\beta = 0$, 10^{-7}, and 10^{-6} cm/W, respectively. The difference is caused by the use of uniform heat generation rate in each element and the element size in the numerical model. When the element size is further reduced, the peak temperatures get closer to the theoretical values with the expense of an increased computational time. Variable time steps are used for the heating and cooling process, and a very small time step is used at the transition from the heating process to the cooling process for numerical stability. An adiabatic analysis is further used to test the amount of energy deposited in the heating model. Under adiabatic conditions, the relative errors between the temperature rise calculated theoretically and that predicted by the finite element model are less than 0.5% for $\beta = 0$, 10^{-7}, and 10^{-6} cm/W.

Results of the Numerical Modeling

The analysis of laser intensity and penetration depth shows that more energy is absorbed near the surface due to the two-photon absorption, which should result in a higher peak temperature at the center of the glass surface. The peak temperature for a single-pulse heating is at the center of the glass surface and can be calculated from Eq. (5-6). The results for various two-photon absorption coefficients at pulse energies from 0.1 to 5 J are shown in Fig. 5-6, where τ_p = 15 ns and D = 0.5 cm. With only one-photon absorption (β = 0), the peak temperature is a linear function of the pulse energy. The nonlinear dependence of the peak temperature on pulse energy is clearly seen with two-photon absorption, especially at low pulse energies. For larger β, the peak temperature increases with the pulse energy much faster and reaches some threshold temperature at much lower pulse energies. The threshold temperature may be determined by the phase transformation temperature, which is between 800 – 1000 K for fused silica. At temperatures greater than the transformation temperature, the glass undergoes a phase transformation from the brittle behavior to viscous-liquid behavior. At Q = 0.5 J, the peak temperature rise is 69 K for β = 0 and 926 K for $\beta = 10^{-5}$ cm/W. The strong two-photon absorption can significantly reduce the damage threshold of the volume-absorbing glass and hence decrease the dynamic range of laser calorimeters. Note that the predicted high temperatures are merely indicative because of the use of constant properties without considering phase transformation. It is important to ensure that the two-photon absorption in the volume-absorbing glass is sufficiently small to prevent damage and to reduce excessive surface heating.

The effect of two-photon absorption on the temperature distribution and history for single- and multiple-pulse laser heating is studied using the axisymmetric model. The temperature histories at the center of the glass surface and center of the glass-copper interface for a single pulse heating are shown in Fig. 5-7, for $\beta = 0$, 10^{-7}, and 10^{-6} cm/W. In all cases, the temperatures increase slowly in the first 20 ns because of the relatively low laser intensity and rapidly from 20 to 40 ns, noting that the peak laser intensity is at $t_m = 2\tau_p = 30\,\text{ns}$. The temperatures change little after 40 ns. For $\beta = 10^{-6}$ cm/W, the maximum temperature rise at the glass surface is more than three times as high as that for $\beta = 0$. At the center of the glass-copper interface, however, the temperature is lower for $\beta = 10^{-6}$ cm/W than for $\beta = 0$. This is because more energy is deposited near the glass surface and the ineffective heat transfer by the glass whose thermal conductivity is small. It can be concluded that the temperature gradient in the glass is increased by the two-photon absorption.

The temperature histories for multiple-pulse heating are shown in Fig. 5-8, where the pulse parameters are the same as those used in Fig. 5-7 with a repetition rate f = 100 Hz. The peak temperature for $\beta = 10^{-6}$ cm/W is much higher than those for $\beta = 0$ and 10^{-7} cm/W and increases as the number of pulses increases. At the beginning of each cooling process, the temperature drops much more for $\beta = 10^{-6}$ cm/W than for the other cases due to heat conduction, as well as convection and radiation losses at the glass surface. The temperature at the center of the glass-copper interface increases slightly during the first 10 pulses. The temperature at the interface is lower for $\beta = 10^{-6}$ cm/W than for the other cases. The excess temperature rise at the glass surface due to the two-photon absorption may cause extra heat loss (by convection and radiation at the surface)

as compared with the volume-absorbing process. The extra heat loss can introduce nonequivalence between the laser heating and the electrical heating; this will subsequently increase the uncertainty of the laser calorimeter.

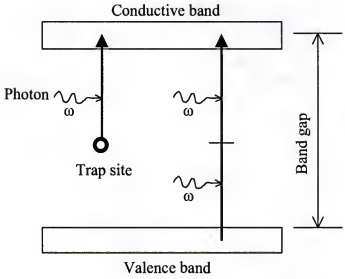

Figure 5-1. Schematic of the band structure of fused silica.

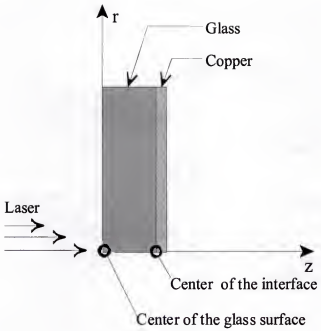

Figure 5-2. Schematic of the thermal model (not to scale).

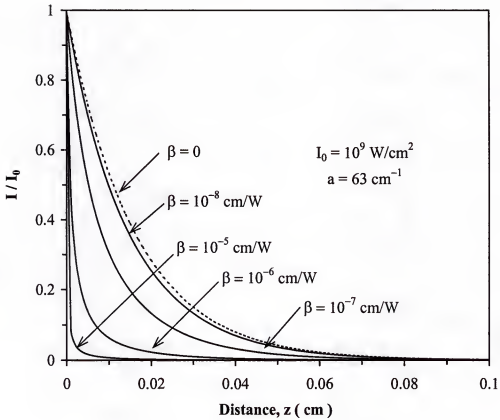

Figure 5-3. Intensity distribution in the z direction
for different two-photon absorption coefficients.

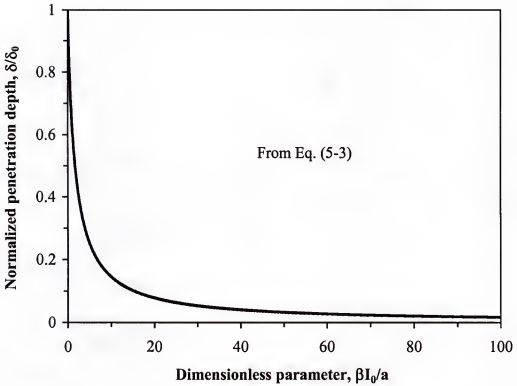

Figure 5-4. The normalized penetration depth as a function of $\beta I_0/a$.

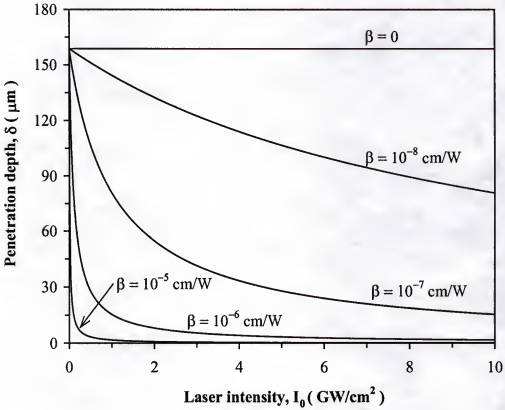

Figure 5-5. The penetration depth versus laser intensity for different two-photon absorption coefficients.

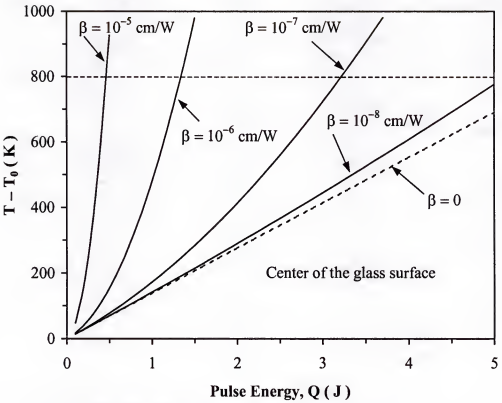

Figure 5-6. Peak temperature rise versus the pulse energy for different two-photon absorption coefficients.

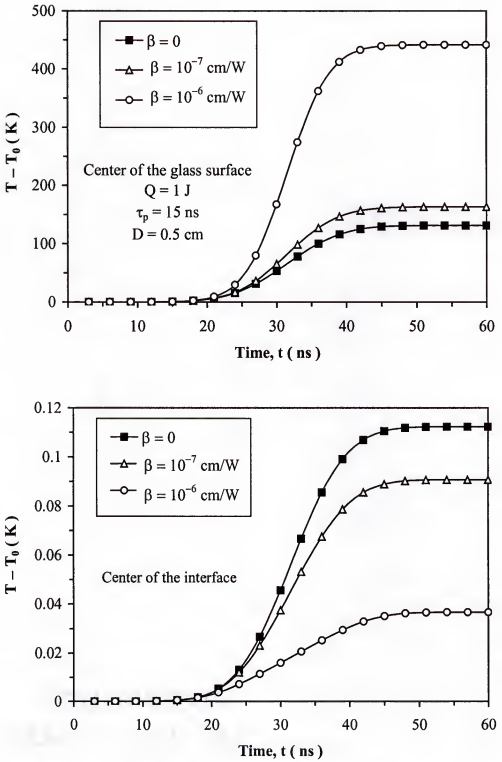
β = 0
β = 10^-7 cm/W
β = 10^-6 cm/W
Center of the glass surface
Q = 1 J
τp = 15 ns
D = 0.5 cm
T – T0 (K)
Time, t (ns)
β = 0
β = 10^-7 cm/W
β = 10^-6 cm/W
Center of the interface
T – T0 (K)
Time, t (ns)

Figure 5-7. Temperature histories for single-pulse heating with two-photon absorption at the center of the glass surface (upper), and center of the glass-copper interface (lower).

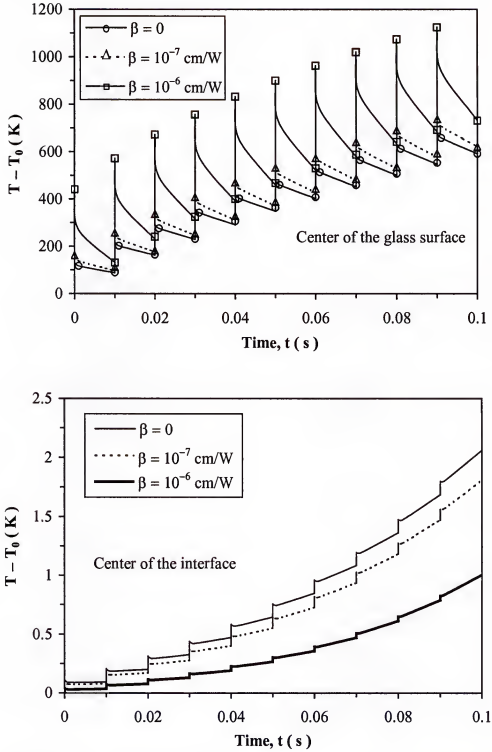

Figure 5-8. Temperature histories for multiple-pulse heating with two-photon absorption at the center of the glass surface (upper), and center of the interface (lower).

CHAPTER 6
PARAMETRIC STUDY OF EXCIMER LASER CALORIMETERS

The goal of this chapter is to gain insight into the heat transfer mechanisms for electrical heating and laser heating. Following the previous model with high pulse energy, the laser heating and electrical heating are modeled under the actual operation conditions with low energy level. This study is helpful to understand the thermal mechanisms in the calorimeter and to improve the future design of calorimeters.

The Finite Element Model

The thermal responses of a thin glass plate with high absorption coefficient and copper is studied under pulsed-laser heating, average-power laser heating, and electrical heating. Because the number of pulses can be up to 4000 in the laser heating, it takes tremendous time to model the transient temperature distribution in the whole calorimeter. Therefore, the axisymmetric finite element model developed in Chapter 4 is adopted for the present study. As shown in Fig. 6-1, the glass plate is assumed circular with a radius of 1.6 cm, only a gold-coated copper disk with the same radius as the glass plate is included, and an electrical heater with 0.25 cm radius is attached to the back of the copper plate. The absorption coefficient of glass is 100 cm^{-1} and the thickness of the glass is 0.05 cm. These are believed to be close to the real values of the glass used in the calorimeter. The thermal conductivity, density, and specific heat of the glass and copper are same as those in Table 4-1. The laser is assumed normally incident on the glass disk.

Furthermore, the temporal distribution of pulse power is considered as a step function instead of the Gaussian distribution for simplification of the modeling of the heating process.

The front surface of glass and the back surface of copper are subject to convection and radiation heat transfer with a convection coefficient of 8 $W/m^2 \cdot K$ (Incropera and DeWitt, 1996) and an emissivity of 0.8 for the glass surface (Touloukian and DeWitt, 1972) and 0.01 for the gold-coated copper surface given by the project leader of NIST. The side surfaces of glass and copper are adiabatic, so that the predicted temperature is the highest. The effect of the side surfaces can be further studied by assuming a convection boundary condition with a convection coefficient from 0 (adiabatic limit) to ∞ (isothermal limit). Three heating methods are considered: pulsed-laser heating for up to 240 pulses, average-power laser heating with the same spatial distribution of the absorbed laser energy, and electrical heating with the average power deposited uniformly over the electrical heater.

For the pulse heating and average-power heating, the heat generation rate in the glass plate caused by the absorbed laser energy can be expressed as (Chen et al., 2000)

$$\dot{q}_1(r,z) = C\ e^{-r^2/b^2} e^{-a \cdot z} \tag{6-1}$$

where r and z are the spatial coordinates, and

$$C = \frac{a(1-R_g)P_a}{\pi b^2} \tag{6-2}$$

where P_a is the average laser power. To model the pulse heating, the average laser power is determined by dividing the energy per pulse (Q) by the FWHM pulse width τ_p because

the laser pulse is modeled as a step function of width τ_p. To model the average-power heating, the laser power is determined by multiplying Q by the pulse repetition rate f. In the electrical heating, the total heating power of $(1-R_g)Q \cdot f$ is uniformly applied to the back surface of the copper within a radius of 0.25 cm.

The reflectivity is 0.04 for normal incidence when the refractive index of glass is taken to be 1.5, indicating that 96% pulse energy is transmitted into and absorbed by the glass. Note that the intensity on the glass-copper interface is less than 1% of the intensity on the glass surface. The reflectance of the glass surface is set to be zero since only the absorbed laser energy is compared with the electrical heating. For typical calibration experiments, τ_p = 15 ns, D = 5 mm, and f = 100 Hz. Various energies per pulse are used in the calibration, from 50 mJ down to 0.01 mJ. For the pulsed-laser heating, the input energy is limited to 12 J and the heating time is limited to 40 s. Hence, the heating time is 40 s for Q < 3 mJ, 12 s for Q = 10 mJ, and 2.4 s for Q = 50 mJ.

The axisymmetric finite element model was built using ANSYS[19] version 5.6 and executed on a 600 MHz personal computer. The element sizes and time steps have been carefully selected and tested to correctly model the laser heating and electrical heating processes within a reasonable amount of computational time. Variable time steps are also used for solution convergence. The initial temperatures of glass and copper are equal to the ambient temperature T_0 = 300 K and the modeling result is represented as the temperature rise $T - T_0$.

Results and Discussion

Laser Heating

For pulsed-laser heating with a pulse energy of 50 mJ and a repetition rate of 100 Hz, the maximum energy of 12 J limits the number of pulses to 240 pulses, which takes only 2.4 s, while the cooling process is modeled up to 40 s. The calculated temperature rises at the centers and edges of the glass surface and copper surface are shown in Fig. 6-2, where G and C denote glass and copper, respectively. The temperature rise is the highest at the center of the glass surface because of the Gaussian distribution (in the r direction) and the exponential decay (in the z direction) of the heat generation rate in the glass. The temperature of the center of the glass surface increases quickly at the beginning and slowly near the end of the heating process (t = 2.4 s), because of the increased heat losses by convection and radiation at the glass surface and heat conduction to other part of the glass and copper. There is a large temperature difference between the G-center and C-center because of the low thermal conductivity of glass. The heat conduction in copper is much larger than that from glass to copper; therefore, the temperature at C-center drops almost at the same time as that of G-center. The temperatures at the edges continue to increase until they reach almost the same temperature as the centers. During and immediately following the heating process, the temperature at the C-edge is slightly higher than that at the G-edge, indicating that heat is transferred from glass to copper near the center and from copper to glass near the edge. At about 8 to 10 s after the power is turned off, the temperature distribution becomes almost one-dimensional, with negligible gradient in the r direction (the temperature gradient in the z direction is also very small). The highest temperature is inside the glass.

The temperatures at the copper surface are slightly higher than those at the glass surface because radiative heat loss is greater at the glass surface.

To study the effect of pulse repetition rate, the pulsed-laser heating with a pulse energy of 50 mJ and a repetition rate of 20 Hz is modeled and shown in Fig. 6-3. Figure 6-3 and Fig. 6-2 show that the temperature rise at the center of the glass surface is much smaller for f = 20 Hz. For each pulse, the temperature rise in the heating process is the same but the cooling process is longer for a lower repetition rate. Hence, the maximum temperature rise is reduced from about 119 K for f = 100 Hz to 37 K for f = 20 Hz.

For pulse energies below 50 mJ, there are 400 to 4000 pulses and the heating process takes up to 40 s. In order to reduce the computational time to a reasonable amount, the heating process is modeled with a average power. The spatial distribution of the heat generation rate is the same as for pulsed-laser heating. During the heating process, the heat generation rate is calculated from Eq. (6-1) with the average power $P_a = Q \cdot f$. This model is validated by comparing with the results for corresponding pulsed-laser heating at Q = 50 mJ. Figure 6-4 shows the temperature histories for average-power laser heating with P_a = 5 W (corresponding to Q = 50 mJ and f = 100 Hz) and P_a = 1 W (corresponding to Q = 50 mJ and f = 20 Hz, or Q = 10 mJ and f = 100 Hz). In the heating process, the temperature at G-center for average-power laser heating lies between the peak and valley of the temperature curve for the corresponding pulse heating. The temperature at C-center is slightly lower for average-power heating than for pulse heating in the initial period, presumably because the higher peak temperatures in the pulse heating process lead to faster heat diffusion. The temperature changes in the cooling process are very similar for both average-power heating and pulse heating.

The temperature histories for the average-power laser heating corresponding to 1 mJ pulse energy are shown in Fig. 6-5a. The power-on period is 40 s with a total energy input of 4 J and the cooling process lasts till 80 s. After the sharp increase of the temperatures at the centers, the temperature gradients in the glass and copper are almost constant in the heating process. At the beginning of the cooling process, the temperatures at the centers drop quickly to almost the same as those at the edges. In the cooling process, the temperature is nearly uniform in the glass and copper. The temperature history for average-power laser heating corresponding to pulse energies below 1 mJ is also studied. The temperature rises at the end of the heating process (t = 40 s) are shown in Fig. 6-5b as functions of the average power. The temperature rise increases linearly when P_a is changed from 1 mW to 100 mW (corresponding to Q = 10 μJ to 1 mJ for f = 100 Hz). Because the maximum temperature at the glass surface is only 304.5 K, the nonlinear effect caused by radiative heat loss is small. The radiative heat transfer coefficient at the glass surface changes from 4.90 to 5.01 $W/m^2 \cdot K$, when the temperature of the glass surface is increased from 300 to 304.5 K.

Electrical Heating

In this study, the heating power is applied to the copper surface as a uniform heat flux with a radius of 0.25 cm to model the electrical heating process. The power and heating time are the same as those for average-power laser heating.

The temperature histories under both convective and radiative boundary conditions for electrical powers of 5 W, 1 W, and 0.1 W are shown in Fig. 6-6. These powers correspond to pulse energies of 50 mJ, 10 mJ, and 1 mJ, respectively, at a

repetition rate of 100 Hz. The peak temperature is at C-center, which is slightly higher than that at G-center. For P_e = 5 W, the temperatures at the centers increase rapidly in the heating process. For P_e = 1 W and 0.1 W, the temperatures at the centers increase rapidly at the beginning of the heating process and then increases gradually as the entire sample heats up. As the cooling process starts, the temperature at the copper surface drops faster than that at the glass surface because of lateral heat diffusion. It is interesting to note that the temperature at C-center actually falls below that at G-center as seen from Fig. 6-6. After the initial cooling period, the temperature gradients in the glass and copper are small and the temperature decreases gradually. The cooling curve is very similar to those for the laser heating.

The comparison between the pulsed-laser heating and the corresponding average-power laser heating indicates they may have the same calibration factors. The different temperature distribution between laser heating and electrical heating suggests the nonequivalence exists for the laser calorimeter. These issues are investigated in the neat two chapters.

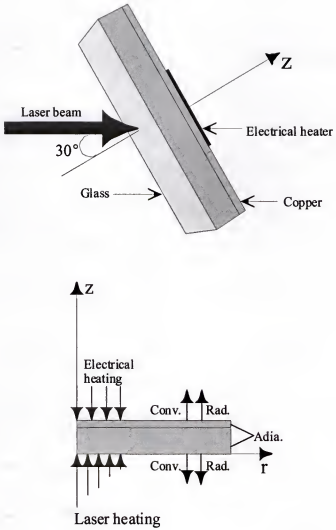

Figure 6-1. Schematic of the end plate of the cavity (upper) and the axisymmetric model (lower).

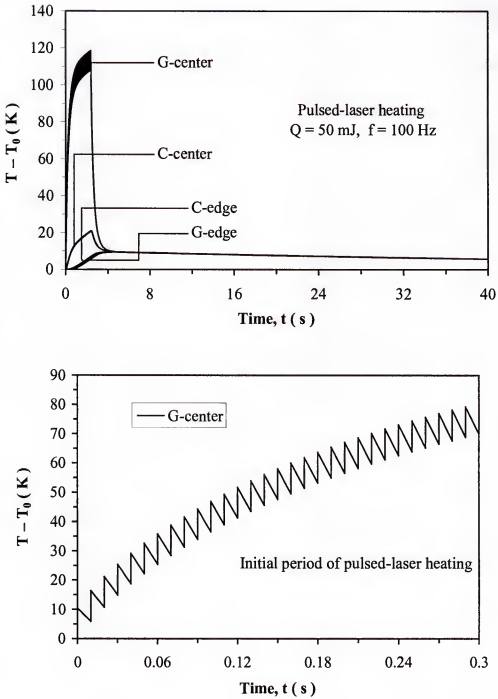

Figure 6-2. Temperature histories for a pulse energy of 50 mJ and a repetition rate of 100 Hz in the heating and cooling process (upper) and the initial heating period (lower).

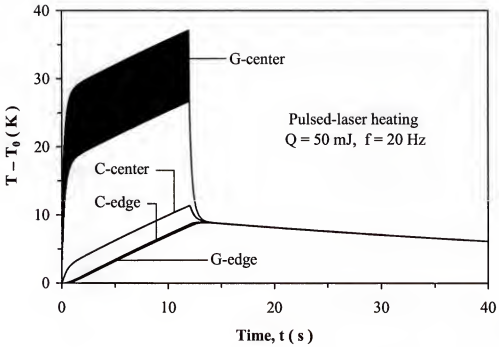

Figure 6-3. Temperature rises for pulsed-laser heating with a repetition rate of 20 Hz.

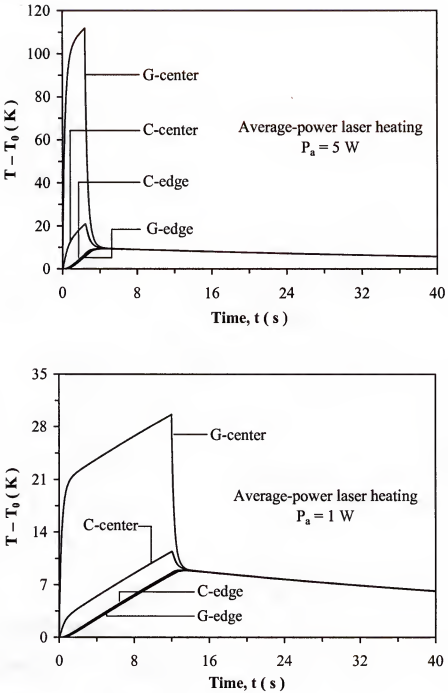

Figure 6-4. Temperature histories for average-power heating with laser powers of (upper) 5 W and (lower) 1 W.

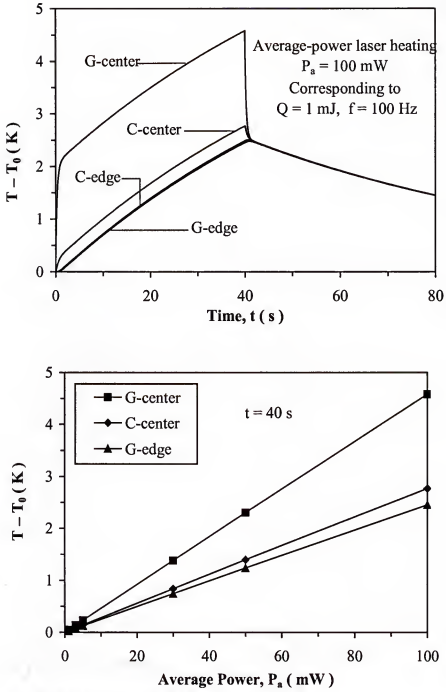

Figure 6-5. (a) Temperature history for average-power heating at a pulse energy of 1 mJ; (b) Temperature rises at 40 s for different pulse energies.

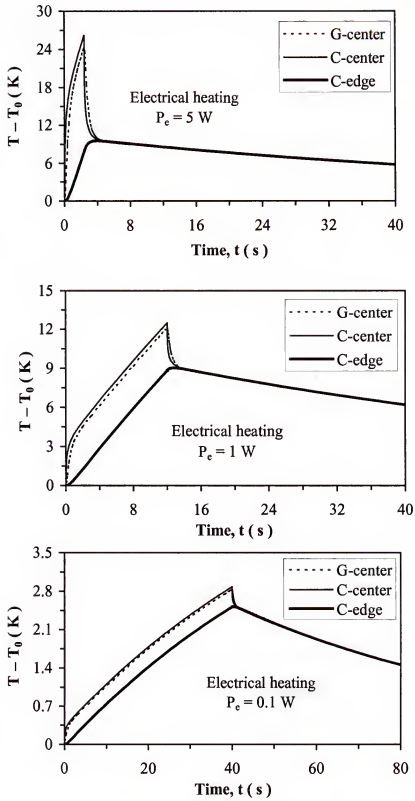

Figure 6-6. Temperature histories for electrical heating with heating powers of 5 W (upper), 1 W (middle), and 0.1 W (lower).

CHAPTER 7
AXISYMETRIC MODELING OF THE CALORIMETER CAVITY

A simplified axisymmetric model of the cavity is built to study the thermal response of the full cavity in the 193 nm pulsed-laser calorimeter. The relative difference between pulsed-laser heating and average-power laser heating is analyzed, and a small relative value between them is predicted. The feasibility of predicting the calibration factor for pulsed-laser heating through the corresponding average-power laser heating is verified. This work is very helpful for the three-dimensional full cavity modeling.

Axisymmetric Model of the Cavity

Calorimeters for measuring energy of 193 nm excimer lasers have been built at NIST. In the 193 nm laser calorimeter, an absorbing cavity made of thin copper plate (about 0.145 mm thick) is suspended in an isothermal heat sink by 4 supports (see Fig. 4-1). The inside surface of the cavity is black painted and the outside surface is gold plated. The end plate of the cavity is tilted at an angle of 60° with respect to the horizontal plane. Two volume-absorbing glass plates (32 mm × 37 mm × 0.5 mm) are epoxied to the inside surfaces of the cavity. An electrical heater with an inner diameter of 11 mm, an outer diameter of 28 mm, and a thickness of 0.5 mm is epoxied to the outside surface of the cavity end. The heater is covered by a heater ring with the same inner and outer diameters, and thickness. Twenty pairs of thermocouples are epoxied to

the cavity and heat sink for measuring the temperature rise of the cavity with respect to the isothermal heat sink.

The absorbing cavity is simplified to an axisymmetric model shown in Fig. 7-1 (Chen and Zhang, 2000). The square glass plate at the back of the cavity (the primary absorber) is simplified to a circular disk and the other glass plate (the secondary absorber) is simplified as a ring, both with the same volume and thickness (0.5 mm). The heat capacity of the gold coating and black paint are added to that of the cavity. Hence, the effective thickness of the cavity is 0.153 cm in the axisymmetric model. Under the principle of the same heat capacity, the inclined rectangular end plate is modeled as a circular axisymmetric disk; the cavity is simplified to a cylindrical shell although the cross-section in the real calorimeter is square. The electrical heater and heater ring with their original dimensions are attached to the cavity end. The supports and thermocouples are neglected in the axisymmetric model for simplification. Hence, the total heat capacity of the simplified axisymmetric model is the same as the sum of the actual cavity, two glass plates, and electrical heater and ring.

Numerical Modeling

The heat conduction path and convection area in the axisymmetric model are approximately the same as those in the actual cavity. The heat transfer from the cavity to the heat sink is through convection and radiation only. The emissivity of the outside gold-plated copper surface is taken to be 0.01. The emissivity of the black paint on the inside surface is 0.86 (McGreer, 1998) and that of the glass surface is 0.8. The view factor of the side surface to the opening is estimated as 0.141 and that from the cavity end

to the opening is estimated as 0.079. Heat transfer within the cavity is dominated by conduction and, therefore, radiative heat transfer between the cavity surfaces is neglected. The convection coefficient is set to be a constant of 8 $W/m^2 \cdot K$, a typical value for natural convection in ambient environment. Initially, the temperatures of the glass and copper are equal to the ambient temperature T_0, which is fixed at 300 K in the present study.

For the pulsed-laser heating and average-power heating, the heat generation rate in the glass plate caused by the absorbed laser energy can be expressed as

$$\dot{q}_l(r,z) = C\ e^{-r^2/b^2} e^{-a \cdot z} \tag{7-1}$$

where r and z are the spatial coordinates, and

$$C = \frac{a(1-R_g)P_a}{\pi b^2} \tag{7-2}$$

where P_a is the average laser power. To model the pulse heating, the average laser power is determined by dividing the energy per pulse (Q) by the FWHM pulse width τ_p because the laser pulse is modeled as a step function of width τ_p. To model average-power laser heating, the laser power is determined by multiplying Q by the pulse repetition rate f.

A thermal model is built based on the Fourier's heat conduction equation using the finite element method. The element sizes and the time steps are carefully selected to yield an acceptable accuracy within a reasonable computational time. The finite element model is further verified under adiabatic conditions, where the final temperature rise is the ratio of the deposited energy to the total heat capacity of the model. For the adiabatic boundary condition, the steady-state temperature rise of the axisymmetric cavity can be easily calculated using Eq. (4-9) in Chapter 4. Notice the reflectance of the glass surface

R_g is set to zero and the total pulse energy E is equal to 12 J. The uniform temperature rise calculated from the Eq. (4-9) is ≈1.411 K. The temperature rises at 200 s predicted by the axisymmetric model for the pulsed-laser heating of 50 mJ pulse energy and the corresponding average-power laser heating are equal to the theoretical value. This indicates that the deposited energies in the modeling for pulsed-laser heating and average-power laser heating are correct.

Results and Analysis

Pulsed-Laser Heating

The temperature history and distribution in the glass and cavity with pulsed-laser heating are studied using the axisymmetric model under both convection and radiation boundary conditions. For pulsed-laser heating with a 50 mJ pulse energy, the maximum energy of 12 J limits the number of pulses to 240 pulses, which takes only 2.4 s. The heat source is turned off at 2.4 s and the modeling extends to 200 s. In the following discussion, the heating process refers to the first 2.4 s and the cooling process refers to the time between 2.4 and 200 s.

The resulting temperature rises at the centers of the glass surface (G-center) and the cavity end (C-center), the edge of the cavity end (C-edge), and the front opening of the cavity (C-front) are shown in Fig. 7-2. The peak temperatures at the centers of the glass surface and the cavity end are smaller than those shown in Fig. 5-2. In the axisymmetric modeling, the heat conduction exists in the copper instead of the adiabatic boundary at the location of the glass edge. In the heating process, the heat is diffused rapidly in the copper cavity because of the large thermal conductivity of the copper.

Hence, the lateral heat conduction in the copper cavity results in a lower peak temperature at the centers. However, the trends of temperature histories at the centers are same as those observed in Fig. 5-2. For example, the temperature at the center of glass surface increases quickly at the beginning and slowly near the end of the heating process and there is a large temperature difference between the centers of the glass and the cavity end. Although the thermal conductivity of the copper is large, the temperature rises at the edge of the cavity end and the front opening of the cavity are small due to the energy loss and big thermal capacity of the cavity. Especially for the front opening of the cavity, the thermal response delays significantly. In the cooling process, the temperature at the front opening of the cavity continues to increase until a nearly uniform temperature has been reached.

Average-Power Laser Heating

The pulsed-laser heating is simplified to the average-power laser heating, in which the heating process is modeled using the average laser power, i.e., modeling laser heating as a continuous power. The heat generation rate is given in Eq. (7-1) during the heating process, where the average power $P_a = Q \cdot f$. For pulsed-laser heating of pulse energy of 50 mJ and repetition rate of 100 Hz, the power for the corresponding average-power heating is 5 W, the heating time is 2.4 s, and the cooling process is up to 200 s. As shown in Fig. 7-3, the maximum temperature rises at the centers of the glass surface and the cavity end are 109.3 K and 17.2 K, respectively. The trend of the temperature in the cooling processes is very similar to that for the corresponding pulsed-laser heating. For example, the temperatures at the centers of the glass surface and the cavity end drop

quickly at the same time; the temperatures at the front opening of the cavity increase slowly until it is equal to those at the centers, and then they drop together.

Relative Difference Analysis

The relative difference N_a of temperature rises for pulsed-laser heating and average-power heating is defined as

$$N_a = \frac{\left|\Delta T_p - \Delta T_a\right|}{\Delta T_a} \cdot 100\% \tag{7-3}$$

where ΔT_p and ΔT_a are temperature rises for pulsed-laser heating and average-power laser heating, respectively. The temperature rises for pulsed-laser heating and average-power laser heating and their relative difference at the center of the cavity end, the edge of the cavity end, and the front opening of the cavity are shown in Figs. 7-4, 5, 6, respectively.

At the center of the cavity end, the maximum temperature rises for pulsed-laser heating and average-power heating are 17.22 K and 17.2 K, whose relative difference is 0.12%. At the beginning of the cooling process, the relative difference drops rapidly and becomes a constant of 0.03% after 40 s. The constant relative difference indicates the temperature decays exponentially after 40 s. The same trend can be observed in Fig. 7-5 and Fig. 7-6. For example, the relative difference changes quickly at the beginning of the cooling process and then it becomes a constant of 0.03%.

The small relative difference lays down the equivalence of the cooling process between the pulsed-laser heating and average-power laser heating with the same deposited energy and heating time. Hence, it is possible to predict the calibration factor

of pulsed-laser heating through modeling its corresponding average-power laser heating for saving computational time of the full cavity modeling. Because the thermocouples are distributed on the sidewall of the cavity, the following discussion is focused on the edge of the cavity end and the front opening of the cavity. Referred to Eq. (2-3), the calibration factor is determined by the deposited energy, temperature difference from t_1 to t_2, cooling constant and the temperature rise integration. The equivalent cooling process indicates the same temperature difference from t_1 to t_2 and the same cooling constant. When times t_1 and t_2 are set to 0 and 200 s, the relative differences of the integration from t_1 to t_2 are 0.03% at the edge of the cavity end and 0.001% at the front opening of the cavity. Even though the time t_2 is reduced to 50 s, the relative differences of the integration are still 0.03%. Although the relative difference of temperature rise in the heating process is larger than that in the cooling process, the integration of temperature rise is almost same. This is because the high temperature in the heating process causes a large energy loss and then results in a low temperature in the cooling process.

Based on the analysis at the edge of the cavity end and the front opening of the cavity, the relative difference of the calibration factor between pulsed-laser heating and average-power laser heating can be estimated as about 0.03% for pulse energy of 50 mJ and repetition rate of 100 Hz. In the actual calibration, the repetition rate of laser pulse is much lower than 100 Hz. The pulsed-laser heating with low repetition rate is closer to the corresponding average-power laser heating than that with high repetition rate, and hence, the equivalence between them becomes better for low repetition rate. The average-power laser heating corresponding to the pulsed-laser heating is used in the full cavity modeling to predict the calibration factor.

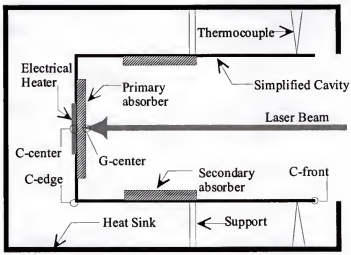

Figure 7-1. Simplified axisymmetric cavity model.

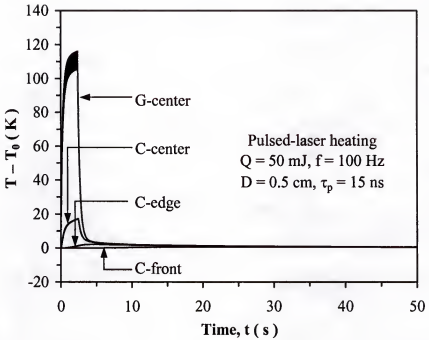

Figure 7-2. Temperature histories for pulsed-laser heating.

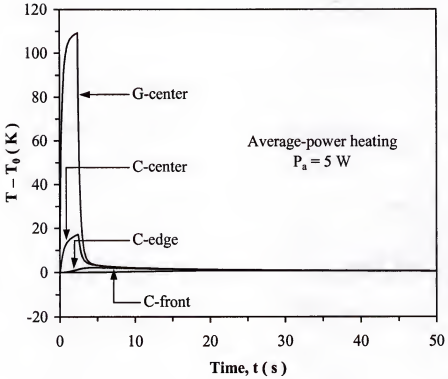

Figure 7-3. Temperature histories for average-power heating.

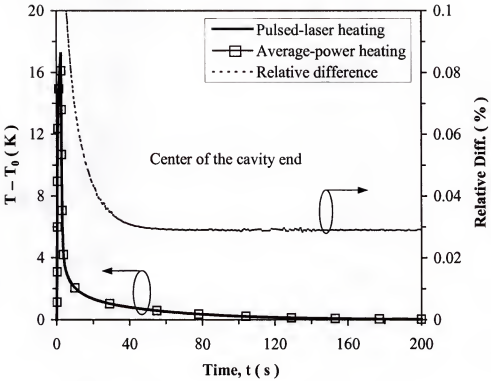

Figure 7-4. Temperature history and relative difference at the center of the cavity end.

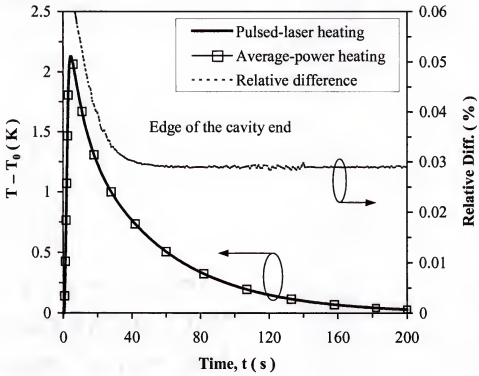

Figure 7-5. Temperature history and relative difference at the edge of the cavity end.

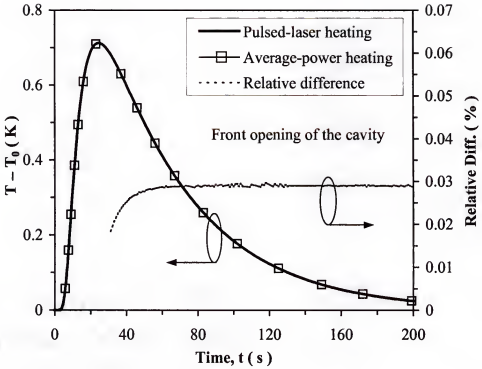

Figure 7-6. Temperature history and relative difference at the front opening of the cavity.

CHAPTER 8
NONEQUIVALENCE ANALYSIS OF LASER CALORIMETERS

Thermal mechanisms of the volume absorber have been studied in the previous chapters. The different heating processes, laser heating and electrical heating cause different calibration factors. The nonequivalence in the calibration factor is very important for the accuracy of pulsed-laser calorimeter. Hence, it is necessary to predict the nonequivalence of the 193 nm laser calorimeter. In this chapter, a three-dimensional finite element model of the full cavity is built and it is used to predict the thermal response at the thermocouple locations for laser heating and electrical heating; the calibration factors are predicted and the nonequivalence of 193 nm laser calorimeter is analyzed.

Thermal Model of the Cavity

Configuration of the Cavity

Nonequivalence analysis is based on the three-dimensional modeling of the full cavity in the 193 nm excimer laser calorimeter which was built at NIST. The 193 nm laser calorimeter is shown in Fig. 8-1. In this calorimeter, the cavity is made of thin copper plate which is approximately 0.0145 cm thick. The cross section of the cavity is 3.528×3.528 cm^2. The inner surfaces of the cavity are black painted for absorbing the radiative energy with a thickness of 25 μm; its mass is about 0.248 g. The outer surfaces are gold plated for limiting the radiation heat transfer and the thickness of the coating is

5 μm. There are two volume-absorbing glass plates inside the cavity for absorbing laser energy; one is epoxied at the back of the cavity and another is attached to the sidewall. The area of each glass plate is 3.2×3.7 cm^2 and the thickness is 0.05 cm. The absorption coefficient of glass is 100 cm^{-1}. The electrical heater is attached to the outside surface of the cavity end. The heater ring is made of copper plate with an inner diameter of 1.1 cm and an outer diameter of 2.8 cm. The surface of the heater ring is also gold plated to reduce radiative heat loss. There is a 0.05 cm gap between the heater ring and the cavity end. The gap is filled with heater wire and thermally conducting epoxy.

The cavity is suspended in the isothermal heat sink through four stainless steel supports. The support is 1.27 cm long; its inner diameter is 0.16 cm and outer diameter is 0.21 cm. The temperature of the cavity is monitored by 20 type-E thermocouples whose conjunctions are epoxied to the outside surface of the cavity sidewall and the isothermal heat sink with a constant temperature of 303 K. Locations of thermocouples on the outside surface of the cavity are shown in Fig. 8-2, in which the circle indicates each conjunction. Because of the different locations, lengths of thermocouple wires are various: 8 thermocouples are 1.27 cm long, 8 thermocouples are 2.54 cm, and 4 thermocouples are 3.81 cm. The sensitivity is 61.391 μV/K; the positive thermoelement is made of Ni-Cr alloy and the negative thermoelement is made of Cu-Ni alloy (Burns et al., 1993).

The important thermophysical properties of stainless steel, gold, Ni-Cr alloy, and Cu-Ni alloy are listed in Table 8-1 (Incropera and DeWitt, 1996; Touloukian and Buyco, 1970; Touloukian et al., 1970). The total hemispherical emissivity is 0.01 for the gold coating and 0.86 for the black paint (McGreer, 1998). The emissivity of the glass is 0.8.

The thermophysical properties of the glass and copper are the same as those listed in Table 4-1. A detail thermal analysis is performed to evaluate the relative magnitude of radiation and convection heat transfer on the inside and outside surfaces of the cavity. The total thermal resistance of 20 thermocouples is 1.8×10^3 K/W and the total thermal resistance of 4 stainless steel is 140 K/W. When the ambient temperature is 300 K and the temperature of the cavity is set to be 310 K, the average natural convection coefficient of the cavity is estimated as 6 $W/m^2 \cdot K$ (Incropera and DeWitt, 1996). The radiative thermal resistances is 1.4×10^3 K/W for the outside surfaces and 14 K/W for inside surfaces. The convective thermal resistance for both the inside surfaces and outside surfaces is 16 K/W. Compared with the convective thermal resistance, the radiation on the outside surfaces and the heat conduction through the thermocouple wires are neglected in the full cavity model.

Three-Dimensional Model

A three-dimensional model of the full cavity is built using finite element software ANSYS 5.6. The gold coating and black paint are so thin that their influence on heat conduction can be neglected; however, they make contribution to the temperature rise of the cavity. Hence, their heat capacities are added to copper plate so that the effective thickness (0.0153 cm) of copper plate is used in the finite element model and the emissivities of the gold coating and black paint are used for the outside surfaces and the inside surfaces of the cavity, respectively. The circular electrical heater and heater ring is simplified to square rings with the same volumes as the original ones.

The meshing of the cavity is shown in Fig. 8-3. Although copper and glass plates are very thin, three-dimensional solid element is used instead of shell element for the glass and copper because of the volumetric heat generation in the glass and electrical heater. The glass and copper plates are divided into several regular volumes for automatic meshing and the adjacent volumes are connected through sharing the nodes on their interface. The conduction bar is used to model the heat conduction through the supports.

The laser beam is incident on the glass surface at the back of the cavity at an incident angle of 30°. The diameter of the laser beam is 0.5 cm. The circular laser beam with uniform intensity in space is simplified to square laser beam with the same cross section area. The reflectance (R_g = 0.04) of the glass surface determines 4% of laser energy is reflected to and absorbed in the glass on the sidewall and 96% of laser energy is transmitted into and absorbed in the glass at the back of the cavity. Because the laser beam is incident on the glass surface inclindly, the transmitted laser beam is not perpendicular to the glass-copper interface. Hence, the tilted volume in which the laser energy is absorbed is generated inside the glass. Based on Eq. 3-11 in Chapter 3, the heat generation rate involved in the full cavity model is given as the following:

$$\dot{q}_1(x, y, z) = C\ e^{-a \cdot z / \cos\theta_2} \tag{8-1}$$

where x, y, and z are the spatial coordinates, and

$$C = \frac{4a(1 - R_g)P_a \cos\theta_1}{\pi D_1^{\,2} \cos\theta_2} \tag{8-2}$$

where a is the absorption coefficient of the glass; D_1 is the laser beam diameter; R_g is the reflectance of the glass surface; P_a is the average laser power, θ_1 is the incident angle, and θ_2 is the refractive angle which is determined using Snell's law. To model average-power laser heating, the laser power is determined by multiplying Q by the pulse repetition rate f. All the reflected energy from the glass at the back of the cavity is considered as uniform heat generation in the glass on the sidewall. The electrical energy is applied through heat generation inside the heater volume, in which the uniform heat generation rate is determined through electrical power divided by the heater volume.

The initial temperature is set to be the ambient temperature (T_0 = 303 K) which is determined by the experimental data. In the modeling, the temperature offset is set to 303 K and hence, the modeling results are the temperature rises corresponding to the ambient temperature. The radiative heat transfer inside the cavity is modeled using radiation matrix method. A space node with the ambient temperature is employed for receiving the radiative energy loss from the inner surface of the cavity. A convection boundary condition is applied on the inside and outside surfaces of the cavity, in which the convection coefficient is temperature dependent.

Available convection correlations fail to predict the convection coefficients in both the heating and cooling processes for the following reasons: (1) the cavity is enclosed by the heat sink with a small distance separating the two; (2) the geometry of the cavity is complicated, which includes tilted, vertical, and horizontal plates; (3) the temperature of the cavity is transient and non-uniform, and the temperature rise is very small. At the beginning of the heating process, thermal diffusion in the nitrogen dominates the heat transfer process. The thermal diffusion length δ_t can be calculated

using $\delta_t = \sqrt{\pi\alpha t}$, and the heat transfer coefficient h can be estimated as $h = k/\delta_t$. The heat transfer coefficient can be initially very high and decreases as the thermal diffusion length increases. Natural convection starts to play a role when boundary layers are formed near the surfaces. Inside the cavity, convection also carries heat from the inclined back plate to the top plate. At the end of the heating process, the nitrogen gas around the cavity has been warmed up. This causes a lower heat transfer coefficient during the cooling process. In the modeling, the convection coefficients are estimated through fitting the experimental results with electrical heating. Even though the temperature distribution and history for average-power laser heating are slightly different from those for the corresponding electrical heating, it is appropriate to use the convection coefficients obtained from electrical heating for the average-power heating because the model employs a linear interpolation. Because the temperature at the heating center is slightly higher for average-power heating than for electrical heating, the convection coefficients obtained from the curve fitting are linearly extended and then used in the average-power laser heating.

Validation of the Numerical Model

The element size and time step have been tested and selected carefully. For the glass plate at the back of the cavity, the element size in the *z* direction is 0.001 cm for $0 \le z \le 0.01$ cm, 0.002 cm for $0.01 \le z \le 0.02$ cm, 0.005 cm for $0.02 \le z \le 0.04$ cm, and 0.01 cm for $0.04 \le z \le 0.05$ cm. Only one layer element is used for the glass at the sidewall and the copper. The element size in x-y plane is 0.2 cm for the center volume with heat generation and 0.4 cm for the other domain. When the element size is reduced by 50%,

the relative difference of the predicted temperature is about 0.8%. Different time steps are used in the heating and cooling process, and very small time steps are used at the beginning of the cooling process for numerical convergence. When every time step is reduced by half, the relative difference of the modeling result is less than 0.1%. Hence, the numerical solutions under the current element sizes and time steps are stable.

The three-dimensional cavity is very complicated. Hence, the mass and deposited energy in the finite element model need to be tested carefully. The total mass of the finite element model is 20.431 g, which is 0.05% less than the theoretical value. The energy deposited in the model is tested through an adiabatic analysis. Under the adiabatic condition, the temperature rise can be calculated using the following equation:

$$\Delta T = \frac{E}{(mc_p)_g + (mc_p)_c + (mc_p)_h + (mc_p)_s} \tag{8-3}$$

where ΔT is the temperature rise at the steady state, E is the total deposited energy in the cavity; $(mc_p)_g$, $(mc_p)_c$, $(mc_p)_h$, and $(mc_p)_s$ are the heat capacities of the glass, cavity, heater, and supports, respectively. For average-power laser heating and electrical heating with deposited energy of 9.022 J, the steady state temperature rises predicted by the adiabatic model are both 1.025 K, which are equal to the value calculated from Eq. (8-3). It indicates that the deposited energies in the finite element model are correct for both average-power laser heating and electrical heating.

Nonequivalence Analysis

Electrical Heating

The experimental data for electrical heating with deposited energies of 9.022 J and 5.008 J are first obtained at NIST. In the experiments, a high-accuracy 6-1/2 digit

(22 bits) digital multimeter (DMM) measures the current through and voltage across the heater. A highly sensitive 7-1/2 digit DMM with a resolution of 0.1 nV measures the thermocouple output voltage. The energy injection time is 80 s, the settling time is 48 s, the final rating period is 120 s, and a sampling interval is 2 s. The integration period is from the initial time ($t_1 = 0$) to the beginning of the final rating period ($t_2 = 128$ s). The standard deviation of the calibration factor in the electrical heating experiments is less than 0.02 % for injection energies of 5 J or greater.

Electrical heating with deposited energies of 9.022 J and 5.008 J, is modeled to fit the experimental results for evaluating the convection coefficients. The energy injection time, the settling time, the final rating period, and the integration period are the same as those in the experiments. The final rating period is used to fit the cooling constant using Eq. (2-1). Based Eq. (2-3), The calibration factor is given as

$$K = \frac{E}{(\Delta T_2 - \Delta T_1) + \eta \int_{t_1}^{t_2} (T(t) - T_0)dt} \qquad (8\text{-}4).$$

Where E is the total deposited energy; ΔT_1 and ΔT_2 are the average temperature rises of 20 thermocouples at times t_1 and t_2, respectively; η is the cooling constant. In the current study, the integration period is from the initial time ($t_1 = 0$) to the beginning of the final rating period ($t_2 = 128$ s). The fitting process is satisfied when the fitted curve agrees well with the experimental curve, the relative difference of the cooling constants is less than 1%, and especially, the relative difference of the calibration factor is less than 0.1%.

The fitted curve and experimental data at the deposited energy of 9.022 J are shown in Fig. 8-4, in which $(T - T_0)$ is the average temperature rises at 20 thermocouple locations. The fitted curve agrees very well with the experimental data. From the fitted

curve, the cooling constant is 0.004352 s^{-1} with a 0.17% relative difference to the experimental value; the calibration factor is 12.4849 J/K and its relative difference to the experimental value is 0.07%. The convection coefficient at the beginning of the heating process is very high because of the small thermal diffusion length. With the development of thermal diffusion, the convection coefficient becomes small and close to the theoretical prediction (2 - 3 $W/m^2 \cdot K$) at the end of the heating process. In the cooling process, the convection coefficient is about 1 $W/m^2 \cdot K$ and changes slightly. It is mostly like heat conduction from cavity surface to the heat sink through the warmed nitrogen. This can be also observed in the experimental data: the cooling constant is almost same when the deposited energy changes from 9 J to 5 J. After linear extension, the convection coefficients obtained by fitting the experimental data are used to model the corresponding average-power laser heating.

The fitted curve and experimental data at the deposited energy of 5.008 J are shown in Fig. 8-5. The fitted curve follows the experimental data very well, especially in the cooling process. The cooling constant is 0.004352 s^{-1}, which is 0.26% larger than the experimental value. The calibration factor predicted from the fitted curve is 12.4610 J/K, which is 0.01% larger than the experimental result.

Average-Power Laser Heating

The convection coefficients attained from fitting the experimental data of the electrical heating with the energies of 9.022 J and 5.008 J are employed to model the corresponding average-power laser heating, respectively. For average-power laser heating, the total deposited energy, the heating time, and the cooling time are same as

those for the corresponding electrical heating. The temperature histories predicted by the three-dimensional model for average-power heating with energies of 9 J and 5 J are shown in Figs. 8-6 and 8-7, respectively. The cooling constant is the same as the corresponding electrical heating. The calibration factors are 12.5371 J/K and 12.5109 J/K for average-power heating with energies of 9.022 J and 5.008 J, respectively.

The nonequivalence is defined as the relative difference of the calibration factors between laser heating and electrical heating. Hence, the nonequivalence N can be calculated using the following

$$N = \frac{|K_a - K_e|}{K_e} \cdot 100\% \tag{8-5}$$

where K_a and K_e are the calibration factors for average-power heating and electrical heating, respectively. Based on Eq. (8-5), the calibration factors predicted by three-dimensional model of the full cavity are used to calculate the nonequivalence between laser heating and electrical heating. The nonequivalence predicted by the full cavity modeling is 0.42% for the deposited energy of 9 J and 0.4% for deposited energy of 5 J. Hence, the nonequivalence of 193 nm laser calorimeter is about 0.4% for the deposited energy from 9 J to 5 J. The nonequivalence predicted by the full cavity model is a good reference for experimentally evaluating the uncertainty of 193 nm laser calorimeter.

Table 8-1. Density, thermal conductivity, and specific heat

	ρ, g/ cm^3	k, W/cm·K	c_p, J/g·K
Gold	19.3	3.17	0.129
Stainless Steel	8.055	0.151	0.48
Ni-Cr alloy	8.6	0.19	0.43
Cu-Ni alloy	8.9	0.23	0.38

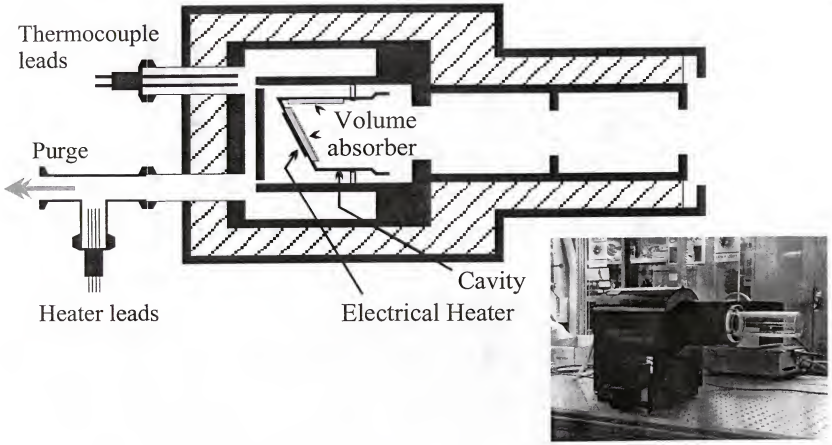

Figure 8-1. 193 nm laser calorimeter.

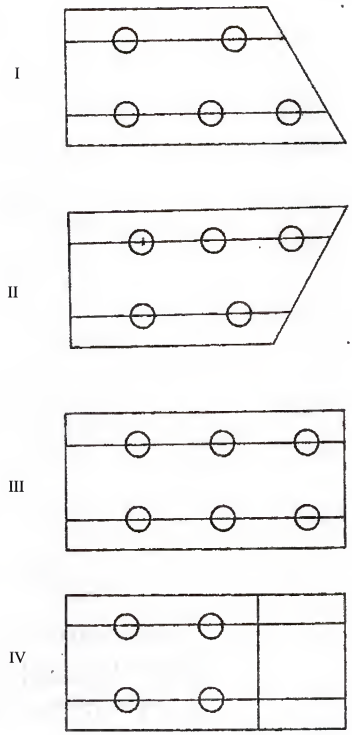

Figure 8-2. Locations of the thermocouples.
(Referring to Fig. 8-1, I and II are the vertical plates, III is the top plate, and IV is the bottom plate.

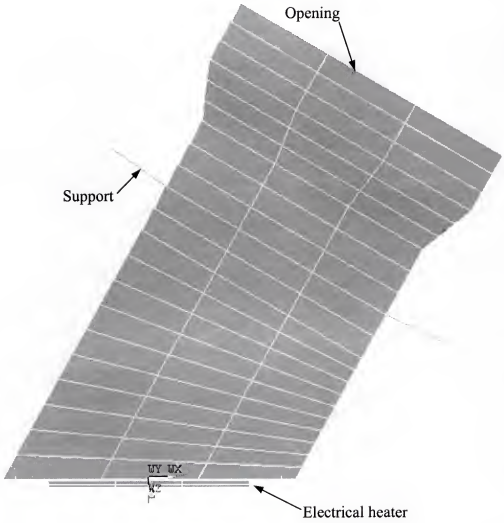

Figure 8-3. Schematic of the cavity meshing.

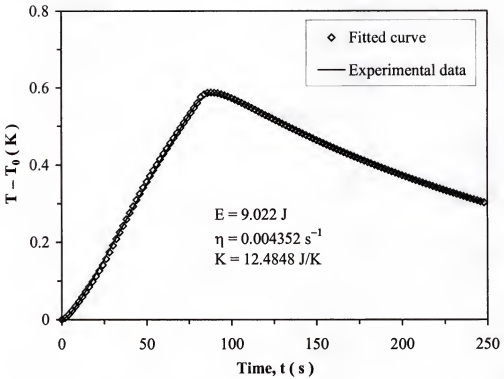

Figure 8-4. Experimental data and fitted curve for the deposited energy of 9 J, where η is the cooling constant and K is the calibration factor for the fitted curve.

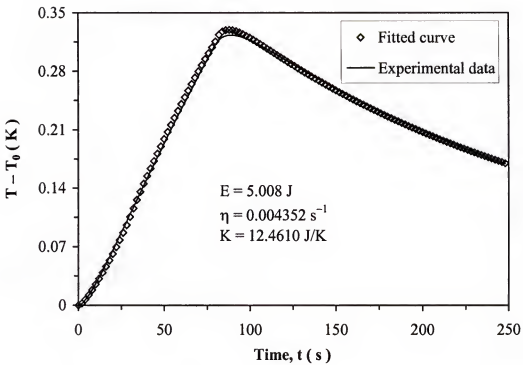

Figure 8-5. Experimental data and fitted curve for the deposited energy of 5 J, where η is the cooling constant and K is the calibration factor for the fitted curve.

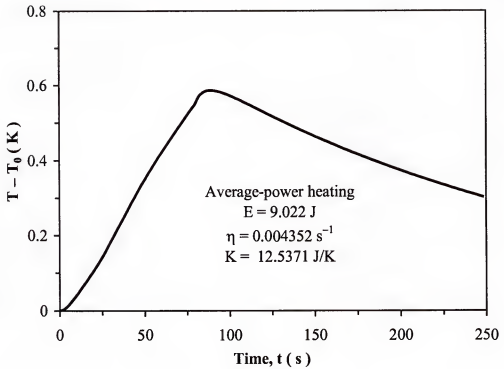

Figure 8-6. Temperature rise for average-power heating at the deposited energy of 9 J.

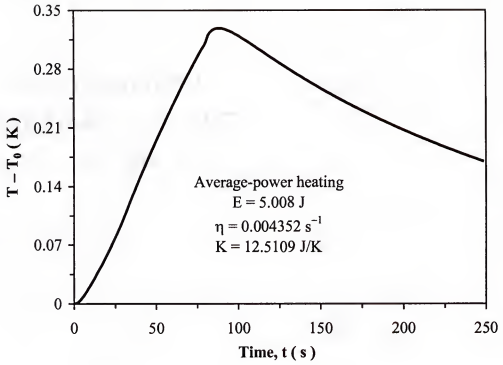

Figure 8-7. Temperature rise for average-power heating at the deposited energy of 5 J.

CHAPTER 9
SUMMARY AND CONCLUSIONS

This dissertation is devoted to an extensive thermal modeling and analysis of the 193 nm excimer laser calorimeter. The thermal mechanisms of the volume absorber under 193 nm excimer laser pulses irradiation have been investigated with one- and multiple-photon absorption. The parametric study has been performed to analyze the thermal responses of pulsed-laser heating, average-power laser heating, and electrical heating. The nonequivalence of the 193 nm laser calorimeter is predicted using the three-dimensional model of the full cavity.

Thermal Mechanisms of the Volume Absorber

The volume-absorbing glass with thickness of 0.1 cm and absorption coefficient of 63 cm^{-1} is analyzed by using three-dimensional and axial-symmetric finite element models. The heating process for a single pulse is almost adiabatic because the heating time is only 120 ns, but the high temperature on the glass surface and low thermal conductivity of glass cause a large energy loss during the laser heating process. The comparison between the tilted incidence and the normal incidence shows the incident angle can reduce the heat flux on the glass surface by increasing the incident area of laser beam and increase the effective absorption length in the glass. In the initial period of the multiple-pulse heating process, temperatures at the center of the glass surface increase

rapidly with the number of pulses. The high peak temperature on the glass surface may limit the number of pulses that can be measured.

A proposed design is presented to reduce the temperature rise on the glass surface and the temperature gradient inside glass, and to accelerate the heat conduction to copper. The maximum temperature rise in the heating process of single pulse moves from the glass surface to the copper surface and it drops rapidly near the end of the heating process when the absorption coefficient of glass drops to below 40 cm^{-1}. For multiple-pulse heating, the peak temperature at the center of the copper surface increases slowly, and that at the center of the glass surface is significantly reduced compared to the previous design. In the laser heating process, the energy loss is smaller for the proposed design than the previous design. Hence, the proposed design may help improve the accuracy and dynamic range of laser calorimeters.

Two-photon absorption in the volume-absorbing glass causes much faster attenuation of the laser intensity than the exponential decay. The penetration depth decreases rapidly with increasing two-photon absorption coefficient and laser intensity, and the volume-absorbing effect can eventually be compressed to surface absorption. For laser heating, two-photon absorption causes a high peak temperature on the glass surface and a large temperature gradient in the glass. Hence, it will reduce the damage threshold and accuracy of pulsed-laser calorimeters. This work provides quantitative information of the two-photon absorption effect in volume-absorbing materials and is important for the future design of laser calorimeters.

Parametric Study of the Laser Calorimeter

Parametric study is performed for the volume-absorbing glass with thickness of 0.05 cm and absorption coefficient of 100 cm^{-1}. The peak temperature for laser heating increases rapidly at the initial heating process and then increases slowly near the end of the heating process because the large energy loss and lateral heat conduction. The temperature at the center of the glass surface for average-power heating goes between the peak value and valley value of the pulsed-laser heating; the temperatures at the center of the copper surface and the edges of the glass and copper for average-power heating are much close to those for pulsed-laser heating especially in the cooling process. This suggests equivalence may exist between the pulsed-laser heating and the average-power laser heating. The maximum temperature at the center of the glass surface is much higher for pulsed-laser heating than for the corresponding electrical heating, and it linearly increases from pulse energy of 0.01 mJ to 1 mJ. The difference in temperature distribution between pulsed-laser heating and electrical heating may introduce nonequivalence to the laser calorimeter.

Nonequivalence of the Laser Calorimeter

The equivalence between pulsed-laser heating and average-power laser heating is further investigated using axial-symmetric model of the cavity. At the edge of the cavity end and the front opening of the cavity, the relative differences of the temperature rise in the cooling process and its integration are about 0.03%. The axial-symmetric modeling establishes the equivalence between the pulsed-laser heating and average-power laser

heating. The average-power laser heating is employed to predict the calibration factor of the 193 nm laser calorimeter instead of the pulsed-laser heating.

The three-dimensional model of the full cavity has been built and used to predict the calibration factors for laser heating and electrical heating. Based on the experimental data of the electrical heating, curve fitting is performed to predict the natural convection coefficients. A high convection coefficient at the initial heating process is predicted due to the small thermal diffusion length and a low convection coefficient for cooling process is observed because the surrounding nitrogen is warmed up. The convection coefficients obtained from the curve fitting are used to model the corresponding average-power laser heating and the calibration factors for laser heating are predicted. The nonequivalence of the 193 nm laser calorimeter is estimated as 0.4% based on the results of the full cavity modeling.

The extensive thermal modeling and analysis presented in this dissertation help understand the pulsed-laser calorimeter deeply. The modeling results indicate that the basic principle used for current pulsed-laser calorimeter is an approximation. Hence, the nonequivalence between the laser heating and the electrical heating is very important for the accuracy of the pulsed-laser calorimeter. In order to reduce the nonequivalence of laser calorimeter, the absorption coefficient and the thickness of the volume absorber should be selected carefully for depositing more laser energy on the copper; the thin-film electrical heater should be used instead of the heater wire; the complicated natural convection should be avoided through creating a vacuum inside the laser calorimeter.

APPENDIX
NOMENCLATURE

a = one-photon absorption coefficient, $4\pi\kappa/\lambda$, cm^{-1}

b = $D/2\sqrt{\ln 2}$, cm

C = heat capacity matrix, J/K

C = constant defined in Eq. (6-2)

C_1 = constant defined in Eq. (3-12)

C_2 = constant defined in Eq. (3-14)

C_3 = constant defined in Eq. (3-16)

c_p = specific heat, J/g·K

D = full width at half maximum (FWHM) beam diameter, cm

E = total input energy, J

f = repetition rate, Hz

h = heat transfer coefficient, $W/cm^2 \cdot K$

I = intensity of laser pulse, W/cm^2

I_0 = transmitted intensity at incident surface, W/cm^2

I_m = peak value of laser intensity, W/cm^2

I_t = transmitted intensity of laser pulse, W/cm^2

K = thermal conductance matrix, W/K

K' = radiation matrix, W/K

K = calibration factor, J/K

k = thermal conductivity, W/cm·K

L = overall thickness of the glass and copper, cm

L_1 = thickness of the glass plate, cm

M = pulse number

N = nonequivalence

N_a = relative difference

n = refractive index

$\tilde{n}$ = complex refractive index

P = laser power, W

P_a = average power of laser pulse, W

P_e = electrical power, W

P_m = peak value of laser power, W

$\dot{\mathbf{Q}}$ = effective heat flow vector, W

$\dot{\mathbf{Q}}_r$ = radiation heat flow, W

Q = energy per pulse, J

q'' = heat flux on the copper surface, W/cm^2

$\dot{q}$ = total heat generation rate, W/cm^3

$\dot{q}_1$ = heat generation rate caused by the transmitted beam, W/cm^3

$\dot{q}_2$ = heat generation rate caused by the reflected beam, W/cm^3

R = reflectance

R_{th} = thermal resistance, K/W

r = distance to the center of the laser beam, cm

$\tilde{r}_{12}$ = complex Fresnel's reflection coefficient

$\mathbf{T}$ = nodal temperature vector, K

$\dot{\mathbf{T}}$ = time derivative vector of nodal temperature, K/s

T = temperature, K

T_0 = ambient temperature, K

T_1 = temperature at initial time t_1 of the single exponential description, K

T_M = temperature of the measuring system, K

T_S = temperature of the surroundings, K

t = time, s

t_1 = time at the beginning of the initial rating period, s

t_2 = time at the beginning of the final rating period, s

t_3 = time at the end of the final rating period, s

t_d = time at the beginning of the power-on period, s

t_e = time at the end of power-on period, s

t_1 = initial time of the single exponential description, s

t_m = time at which the pulse power is maximum, s

t_p = time at the peak output voltage, s

x,y,z = coordinates, cm

Greek Symbols

ΔT = temperature rise, K

α = thermal diffusivity, cm^2/s

β = two-photon absorption coefficient, cm/W

δ = penetration depth, cm

δ_0 = penetration depth with only single-photon absorption, cm

δ_t = thermal diffusion length, cm

ε = total hemispherical emissivity

η = cooling constant, s^{-1}

θ_1 = angle of incidence, degree

θ_2 = angle of refraction, degree

κ = extinction coefficient

λ = wavelength in vacuum, μm

ρ = density, g/cm^3

σ = Stefan-Boltzmann constant, 5.67×10^{-12} $W/cm^2 \cdot K^4$

τ = $\tau_p / 2\sqrt{\ln 2}$, s

τ_p = FWHM pulse width, s

υ = speed of sound, m/s

ℓ = path length, cm

Subscripts

a = average-power laser heating

air = air

c = copper

e = electrical heating

g = glass

p = pulsed-laser heating

REFERENCES

Angelucci, N., and Bianco, N., 1997, "Thermal Transient Analysis of Thin Film Multilayers Heated by Pulsed Laser," *International Journal of Heat and Mass Transfer*, Vol. 40, pp. 4487-4491.

Brimacombe, R.K., Taylor, R.S., and Leopold, K.E., 1989, "Dependence of the Nonlinear Transmission Properties of Fused Silica Fibers on Excimer Laser Wavelength," *Journal of Applied Physics*, Vol. 66, pp. 4035-4040.

Brown, H.D. (Ed.), 1969, *Biochemical Microcalorimetry*, Academic Press, Inc., New York.

Burns, G. W., Scroger, M. G., Strouse, G. F.,Croarkin, M. C., and Guthrie, W. F., 1993, *Temperature-Electromotive Force Reference Functions and Tables for the Letter-Designated Thermocouple Types Based on the ITS-90*, U. S. Government Printing Office, Washington, DC.

Chen, D.H., Dowell, M.L., Cromer, C.L., and Zhang, Z.M., 2000, "Thermal Modeling of Calorimeters for Excimer Lasers at 193 nm Wavelength," presented at the *34th AIAA Thermophysics Conference*, Denver, CO, June 19-22, AIAA paper No. 2000-2367.

Chen, D.H., and Zhang, Z.M., 2000, "Thermal Analysis of the Volume Absorber in Pulsed Excimer Laser Calorimeters," *International Journal of Heat and Mass Transfer*, Vol. 43, pp. 3061-3072.

Chen, D.H., and Zhang, Z.M., 2000, "Thermal Modeling of the Cavity in Pulsed Excimer Laser Calorimeter," presented at the *International Mechanical Engineering Congress and Exposition* (IMECE), Orlando, FL, November 5-10, ASME HTD-Vol. 366-5, pp.183-186.

El-Adawi, M.K., Abdel-Naby, M.A., and Shalaby, S.A., 1995, "Laser Heating of A Two-Layer System with Constant Surface Absorption: An Exact Solution," *International Journal of Heat and Mass Transfer*, Vol. 38, pp. 947-952.

Franzen, D.L., and Schmidt, L.B., 1976, "Absolute Reference Calorimeter for Measuring High Power Laser Pulses," *Applied Optics*, Vol. 15, pp. 3115-3122.

Fushinobu, K., Kimizuka, J., Satoh, I., and Kurosaki, Y., 1996, "Heat Transfer Characteristics in Polymers with Excimer Laser Irradiation," *Transport Phenomena in Materials Processing and Manufacturing*, ASME-HTD, Vol. 336, pp. 39-44.

Ganesh, R.K., and Faghri, A., 1997, "A Generalized Thermal Modeling for Laser Drilling Process—I. Mathematical Modeling and Numerical Methodology," *International Journal of Heat and Mass Transfer*, Vol. 40, pp. 3351-3360.

Grigoropoulos, C.P., Park, H.K., and Xu, X., 1993, "Modeling of Pulsed Laser Irradiation of Thin Silicon Layers," *International Journal of Heat and Mass Transfer*, Vol. 36, pp. 919-924.

Himminger, W., and Höhne, G (Eds.), 1984, *Calorimetry-Fundamentals and Practice*, Verlag Chemie GmbH, D-6940 Weinheim.

Honner, M., and Kunes, J., 1999, "On the Wave Diffusion and Parallel Nonequilibrium Heat Conduction," *Journal of Heat Transfer*, Vol. 121, pp. 702-707.

Incropera, F.P., and DeWitt, D.P., 1996, *Fundamentals of Heat and Mass Transfer*, 4th ed., Wiley, New York.

Joseph, D. D., and Preziosi, L., 1989, "Heat Waves," *Reviews of Modern Physics*, Vol. 61, pp. 41-73.

Kingery, W.D., 1959, *Property Measurements at High Temperatures*, Wiley, New York.

Kittelmann, O., and Ringling, J., 1994, "Intensity-Dependent Transmission Properties of Window Materials at 193-nm Irradiation," *Optics Letters*, Vol. 19, pp. 2053-2055.

Kohnke, P. (Ed.), 1997, *ANSYS Theory Reference Release 5.4*, 8th Ed., ANSYS, Inc., Canonsburg, PA.

Leonhardt, R.W., 1998, "Calibration Service for Laser Power and Energy at 248 nm," *NIST Technical Note 1394*, U.S. Government Printing Office, Washington.

Leonhardt, R.W., and Scott, T.R., 1995, "Deep-UV Excimer Laser Measurements at NIST," *Proceedings SPIE*, Vol. 2439, pp. 448-459.

Longtin, J.P., and Tien, C.L., 1997, "Efficient Laser Heating of Transparent Liquids Using Multiphoton Absorption," *International Journal of Heat and Mass Transfer*, Vol. 40, pp. 951-959.

Mann, K., Apel, O., and Eva, E., 1998, "Characterization of Absorption and Scatter Losses on Optical Components for ArF Excimer Lasers," *SPIE Proceedings*, Vol. 3578, pp. 614-624.

McCullough, J.P., and Scott, D.W. (Eds.), 1968, *Experimental Thermodynamics*, Vol. 1, Plenum Press, New York.

McGahan, W.A., and Cole, K.D., 1992, "Solutions of the Heat Conduction Equation in Multilayers for Photothermal Deflection Experiments," *Journal of Applied Physics*, Vol. 72, pp. 1362-1373.

McGreer, M., 1998, *Total Emittance Test Report*, DSET Labs Inc, Phoenix, AZ.

Özisik, M.N., and Tzou, D.Y., 1994, "On the Wave Theory in Heat Conduction," *Journal of Heat Transfer*, Vol. 116, pp. 526-535.

Palik, E.D., 1985, *Handbook of Optical Constants of Solids,* Academic Press, Inc., Orlando, FL.

Pätzel, R., 1999, "An Introduction to Excimer Lasers," *The Photonics Design and Applications Handbook*, Book 3, 45th Ed., pp. 194-199.

Qiu, T.Q., Juhasz, T., Suarez, C., Bron, W.E., and Tien, C.L., 1994, "Femtosecond Laser Heating of Multi-Layer Metals–II. Experiments," *International Journal of Heat and Mass Transfer*, Vol. 37, pp. 2799-2808.

Qiu, T.Q., and Tien, C.L., 1992, "Short-Pulse Laser Heating on Metals," *International Journal of Heat and Mass Transfer*, Vol. 35, pp. 719-726.

Qiu, T.Q., and Tien, C.L., 1994, "Femtosecond Laser Heating of Multi-Layer Metals–I. Analysis," *International Journal of Heat and Mass Transfer*, Vol. 37, pp. 2789-2797.

Rothschild, M., Forte, A.R., Kunz, R.R., Palmateer, S.C., and Sedlacek, J.H.C., 1997, "Lithography at a Wavelength of 193 nm," *IBM Journal of Research and Development*, Vol. 41, pp. 49-54.

Scott, T.R., 1988, "NBS Laser Power and Energy Measurements," Laser Beam Radiometry, A.A. Sanders ed., *Proceedings SPIE*, Vol. 888, pp. 48-54.

Seward III, T.P., Smith, C., Borrelli, N.F., and Allan, D.C., 1997, "Densification of Synthetic Fused Silica Under Ultraviolet Irradiation," *Journal of Non-Crystalline Solids*, Vol. 222, pp. 407-414.

Siegel, R., and Howell, J.R., 1992, *Thermal Radiation Heat Transfer*, 3rd ed., Hemisphere Publishing Corp., Washington.

Skinner, H.A. (Ed.), 1962, *Experimental Thermochemistry*, Vol. 2, Interscience Publishers, New York.

Svelto, O., 1998, *Principles of Lasers*, 4th Ed., Plenum Press, New York and London.

Taylor, A.J., Gibson, R.B., and Roberts, J.P., 1988, "Two-Photon Absorption at 248 nm in Ultraviolet Window Materials," *Optics Letters*, Vol. 13, pp. 814-816.

Touloukian, Y.S., and Buyco, E.H., 1970, Specific heat: metallic elements and alloys, *Thermophysical Properties of Matter*, Vol. 4, IFI/Plenum, New York.

Touloukian, Y.S., and Dewitt, D.P., 1972, Thermal radiative properties: nonmetallic solids, *Thermophysical Properties of Matter*, Vol. 8, IFI/Plenum, New York.

Touloukian, Y.S., Powell, R.W., Ho, C.Y., and Klemens, P.G., 1970, Thermal conductivity: metallic elements and alloys, *Thermophysical Properties of Matter*, Vol. 1, IFI/Plenum, New York.

Vedavarz, A., Mitra, K, and Kumar, S., 1994, "Hyperbolic Temperature Profiles for Laser Surface Interactions," *Journal of Applied Physics*, Vol. 76, pp. 5014-5021.

Weast, R. C., and Astle, M. J. (Eds.), 1981, *CRC Handbook of Chemistry and Physics*, 60th Ed., CRC Press, Inc., Boca Raton, FL.

Weitzman, P.S., and Osterberg, U., 1996, "Two-Photon Absorption and Photoconductivity in Photosensitive Glasses," *Journal of Applied Physics*, Vol. 79, pp. 8648-8655.

West, E.D., and Case, W.E., 1974, "Current Status of NBS Low-Power Laser Energy Measurement," *IEEE Transactions on Instrumentation and Measurement*, Vol. IM-23, pp. 422-425.

West, E.D., Case, W.E., Rasmussen, A.L., and Schmidt, L.B., 1972, "A Reference Calorimeter for Laser Energy Measurements," *Journal of Research of the National Bureau of Standards*, Vol. 76A, pp. 13-26.

West, E.D., and Churney, K.L., 1970, "Theory of Isoperibol Calorimetry for Laser Power and Energy Measurements," *Journal of Applied Physics*, Vol. 41, pp. 2705-2712.

White, W.P., 1928, *The Modern Calorimeter*, Reinhold Publishing Corp., New York.

Xu, X., Grigoropoulos, C.P., Russo, R.E., 1995, "Heat Transfer in Excimer Laser Melting of Thin Polysilicon Layers," *Journal of Heat Transfer*, Vol. 117, pp. 708-715.

Xu, X., and Song, K.H., 1997, "Radiative Transfer in Pulsed-Laser-Induced Plasma," *Journal of Heat Transfer*, Vol. 119, pp. 502-508.

Zhang, Z.M., and Chen, D.H., 2001, "Thermal Analysis of Multiphoton Absorption at 193 nm in Volume-Absorbing Glass," accepted for presentation at the *35th National Heat Transfer Conference*, Anaheim, CA, June 10-12.

Zhang, Z.M., Livigni, D.J., Jones, R.D., and Scott, T.R., 1996, "Thermal Modeling and Analysis of Laser Calorimeters," *Journal of Thermophysics and Heat Transfer*, Vol. 10, pp. 350-356.

BIOGRAPHICAL SKETCH

Donghai Chen was born in Heilongjiang Province, PR China. He received his Bachelor of Engineering with honors and Diploma of Business Administration from Tsinghua University in July 1992. He was directly admitted to the Graduate School of Tsinghua University and received a master's degree in July 1994. After graduation, he continued to work in Tsinghua University for almost 3 years. At Tsinghua University, he worked on the optical diagnostics of temperature for turbine blades and combustion products in gas turbine.

He came to the University of Florida for his doctoral studies in the fall of 1997. While attending the University of Florida, he worked on the thermal modeling and analysis of 193 nm pulsed excimer laser calorimeters, served as a teaching assistant for the Heat Transfer II course for 6 semesters, and received Best Student Authored Paper Award from the Department of Mechanical Engineering and Academic Achievement Award for International Students from the Office of International Studies and Programs. In the summer of 1999, he worked at the National Institute of Standards and Technology, performing thermal modeling and experimental studies for the 193 nm laser power/energy calibration system.

In leisure, he enjoys outdoor activities and sports. He wishes to pursue a career in applied heat transfer technology.

I certify that I have read this study and that in my opinion it conforms to acceptable standards of scholarly presentation and is fully adequate, in scope and quality, as a dissertation for the degree of Doctor of Philosophy.

Zhuomin Zhang, Chairman
Associate Professor of Mechanical Engineering

I certify that I have read this study and that in my opinion it conforms to acceptable standards of scholarly presentation and is fully adequate, in scope and quality, as a dissertation for the degree of Doctor of Philosophy.

Jacob N. Chung
Eminent Scholar of Mechanical Engineering

I certify that I have read this study and that in my opinion it conforms to acceptable standards of scholarly presentation and is fully adequate, in scope and quality, as a dissertation for the degree of Doctor of Philosophy.

David W. Hahn
Assistant Professor of Mechanical Engineering

I certify that I have read this study and that in my opinion it conforms to acceptable standards of scholarly presentation and is fully adequate, in scope and quality, as a dissertation for the degree of Doctor of Philosophy.

Jill E. Peterson
Associate Professor of Mechanical Engineering

I certify that I have read this study and that in my opinion it conforms to acceptable standards of scholarly presentation and is fully adequate, in scope and quality, as a dissertation for the degree of Doctor of Philosophy.

David B. Tanner
Professor of Physics

This dissertation was submitted to the Graduate Faculty of the College of Engineering and to the Graduate School and was accepted as partial fulfillment of the requirements for the degree of Doctor of Philosophy.

May 2001

M. J. Ohanian
Dean, College of Engineering

Winfred M. Phillips
Dean, Graduate School